ADVANCED ENERGY MATERIALS
www.advenergymat.de

Recent Advances in Engineered Ru-Based Electrocatalysts for the Hydrogen/Oxygen Conversion Reactions

Xianjun Cao, Juanjuan Huo, Lu Li, Junpeng Qu, Yufei Zhao, Weihua Chen, Chuntai Liu, Hao Liu,* and Guoxiu Wang**

The application of renewable energy conversion devices is considered as one of the effective ways to alleviate the energy shortage and environmental pollution. Designing electrocatalysts with excellent performance and affordable price is promising to accelerate the reaction process and large-scale application. At present, ruthenium (Ru)-based nanomaterials have shown similar catalytic activity but superior price demand compared to commercial Pt/C. This undoubtedly makes Ru-based nanomaterials a perfect candidate to replace advanced Pt catalysts. Significant progress is made in the rational design of Ru-based electrocatalysts, but an in-depth understanding of the engineering strategies and induced effects is still at an early stage. This review summarizes the modification strategies for enhancing the catalytic activity of Ru, including surface structure, metal element, nonmetal element, size, bimetallic oxides, and heterostructure engineering strategies. Then the induced electronic modulation effects generated by the intramolecular and intermolecular of the Ru-based nanomaterials are elucidated. Further, the application progress of engineered Ru-based nanomaterials for hydrogen and oxygen conversion reactions is highlighted, and the correlations of engineering strategies, catalytic activity, and reaction pathways are elaborated. Finally, challenges and prospects are presented for the future development and practical application of Ru-based nanomaterials.

1. Introduction

The excessive consumption of non-renewable fossil fuels causes severe worldwide problems of energy shortage and environmental pollution. Therefore, it is important to pursue green and clean energy as candidates to mitigate the energy crisis and global warming.[1–5] Hydrogen with high specific energy density produced by water electrolysis devices is promising to store renewable and sustainable energy.[6,7] The oxygen evolution reaction (OER) occurs at the anode of the water electrolysis device and needs to be driven at a high overpotential, which severely limits the overall efficiency of H_2 production. Fuel cells have also been widely studied due to their high energy density, high energy conversion rate, and environmental friendliness. Fuel cells, including anion exchange membrane fuel cell (AEMFC), zinc–air fuel cell (Zn–air battery), undergo oxygen reduction reaction (ORR) at the cathode, and hydrogen oxidation reaction (HOR) and OER occur at the anodes, respectively.[8–11] The electrocatalytic activity of the aforementioned hydrogen evolution reaction (HER), OER, ORR, and HOR are closely dependent on the nature of the electrocatalysts. Therefore, the selection of suitable and highly efficient electrocatalysts to accelerate these reactions is crucial for future commercial applications of electrochemical conversion devices.[12]

Precious metal platinum (Pt) is regarded as the "Holy Grail" for hydrogen–oxygen energy conversion reactions, exhibiting excellent catalytic activity and stability.[13,14] However, the high price is the main obstacle impeding the large-scale implementation. Recently, ruthenium (Ru) has been investigated as one of the promising candidates to replace Pt with relatively low cost (only 6–36% of Pt).[15,16] In 1926, it was the first time discovered that a small amount of ruthenium chloride could oxidize the mixture of hydrobromic acid and perchloric acid to bromine.[17] Then, Ru-based electrocatalysts have revealed vital electrocatalytic performance for both reduction and oxidation reactions. For instance, Ru(IV) has been extensively studied as catalysts for OER.[18–20] However, over-oxidizing RuO_2 to higher oxides ($RuO_2 + 2H_2O \rightarrow RuO_4\ (aq) + 4H^+ + 4e^-$) at high OER overpotentials leads to the dissociation of RuO_2 and the reduced catalytic activity.[21] Ru-based catalysts for HER have been

X. Cao, J. Huo, L. Li, J. Qu, Y. Zhao, H. Liu
Joint International Laboratory on Environmental and Energy Frontier Materials
School of Environmental and Chemical Engineering
Shanghai University
Shanghai 200444, P. R. China
E-mail: yufei-zhao@shu.edu.cn; hao.liu@uts.edu.au

W. Chen, C. Liu
Key Laboratory of Materials Processing and Mold (Zhengzhou University)
Ministry of Education
Zhengzhou 450002, P. R. China

H. Liu, G. Wang
Centre for Clean Energy Technology
Faculty of Science
University of Technology Sydney
Broadway, Sydney, NSW 2007, Australia
E-mail: guoxiu.wang@uts.edu.au

The ORCID identification number(s) for the author(s) of this article can be found under https://doi.org/10.1002/aenm.202202119.

DOI: 10.1002/aenm.202202119

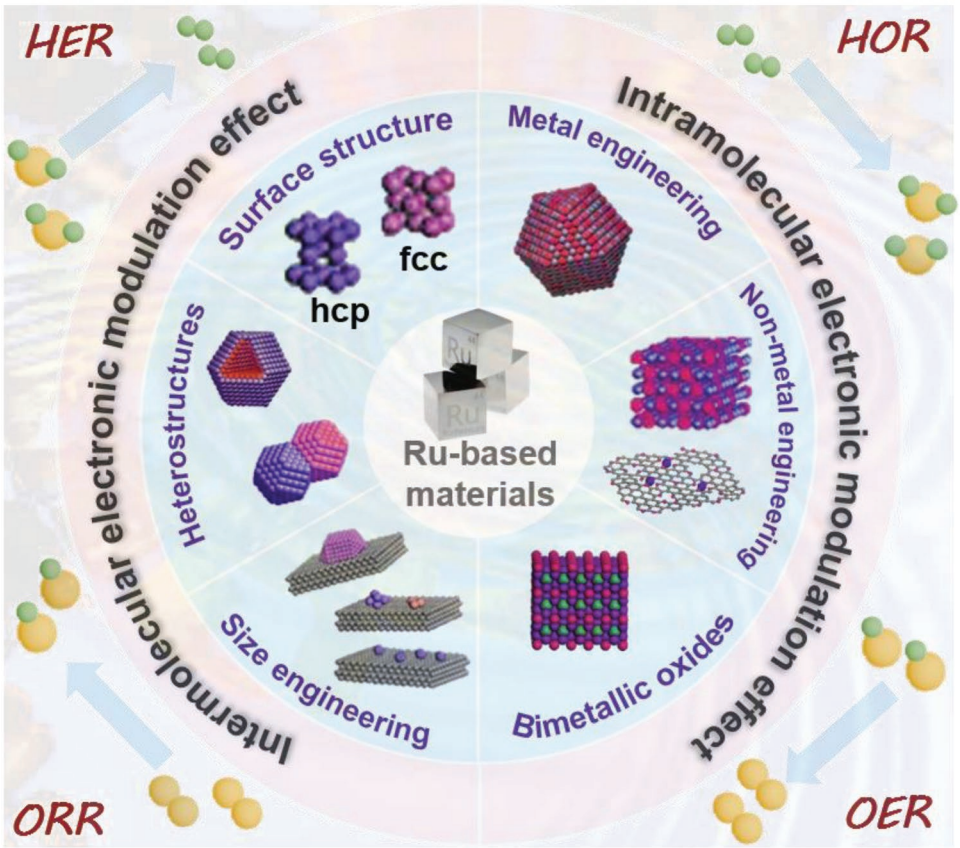

Figure 1. Modification strategies for Ru-based materials. Schematic illustration of various Ru-based catalyst development strategies, resulting in electronic modulation effects to promote renewable energy conversion reactions, including HER, HOR, ORR, and OER.

studied referring to the 1970s, and the metallic Ru was found to have a similar H-binding strength (65 kcal mol^{-1}) to Pt, which laid a theoretical foundation for designing Ru-based HER electrocatalysts. Furthermore, the strong oxophilicity properties of Ru makes it favorable for the preferential adsorption of OH* and O_2 to promote HOR and ORR processes, respectively.[22–25] Therefore, considerable efforts and strategies have been devoted to developing Ru-based nanomaterials with specific properties and excellent catalytic capability. It is demonstrated that the combination of Ru with the chalcogen Se resulted in the electron transfer from Ru to Se, which increased the ORR catalytic activity.[26,27] Furthermore, increasing the crystallinity of metallic Ru was considered to be an effective way to promote the HER and designing Ru single atoms embedded carbon substrates maximized the atom utilization and promoted the ORR catalytic activity.[28,29]

Previously, there are some excellent review articles related to Ru-based materials for water splitting have been reported, covering the preparation, characterization methods to the impacts of the modification strategies on the catalytic activity.[30–34] However, a comprehensive and systematical review regarding the engineering strategies and the corresponding electron modulation effects of Ru-based electrocatalysts for hydrogen/oxygen conversion reactions, including HER, OER, ORR, and HOR, is lacking and desired. Herein, we review the latest research progress of Ru-based electrocatalysts for the above energy conversion reactions and provide an overview of the relationship between the engineering strategies and catalytic performance (**Figure 1**). First, the engineering strategies for the Ru-based nanomaterials are discussed, including surface structure engineering, metal element engineering, nonmetal element engineering, size engineering, bimetallic oxides, and heterostructure engineering strategies. Then, the corresponding electron modulation effects induced by the engineering strategies will be summarized. In addition, we will focus on the Ru-based catalysts with desired engineering strategies and enhanced mechanisms in HER, HOR, ORR, and OER electrocatalytic reactions. The fundamental insights can provide guidance in designing high-performance catalysts for electrocatalysis. Finally, the research challenges and future application prospects of Ru-based electrocatalysts are highlighted.

2. Engineering Strategies of Ru-Based Materials

The modification of Ru-based materials can effectively tune the electronic structure, which not only optimizes the binding energy to reactants/intermediates, but also lowers the reaction energy barrier of the rate-limiting step. Therefore, proper engineering strategies developed for Ru-based materials are helpful in exerting the corresponding catalytic activity. This

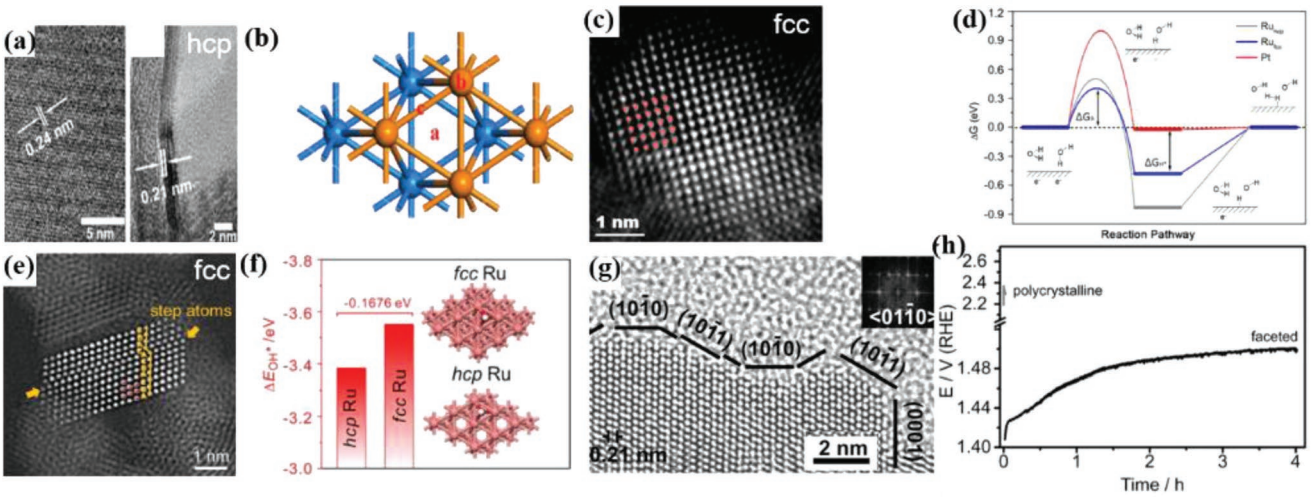

Figure 2. a) High-resolution transmission electron microscope (HR-TEM) image of fcc Ru NSs. b) Schematic diagram of different adsorption sites on Ru(001) surface; a-hollow sites; b-top sites; c-bridging sites. Reproduced with permission.[39] Copyright 2016, American Chemical Society. c) High-angle annular dark-field scanning transmission electron microscopy (HAADF-STEM) image of fcc Ru NPs. d) Gibbs free energy diagrams of HER in different structures of Ru and Pt. Reproduced with permission.[42] Copyright 2016, American Chemical Society. e) HAADF-STEM images of fcc Ru nanoparticles with stacking fault structures. f) Binding energies of OH* on fcc and hcp Ru surfaces. Reproduced with permission.[43] Copyright 2021, Elsevier. g) HR-TEM image of Ru branches and fast Fourier transform (inset). h) Chronopotentiometry (CP) curves of Ru branches (black) and polycrystalline nanoparticles (gray) in 0.1 M $HClO_4$. Reproduced with permission.[46] Copyright 2020, Wiley-VCH.

section will discuss the modification of Ru-based materials from the following five aspects: 1) surface structure engineering strategies, adjusting the crystal structure results in the rearrangement of surface Ru atoms and the adsorption ability of active intermediates; 2) metal element engineering strategies, alloying with other metals improves the intrinsic activity of Ru catalysts due to the charge redistribution; 3) nonmetal element engineering strategies, the introduction of nonmetal (O, P, and B) element to accept the excess electrons from Ru reduces the reaction energy barrier of electrocatalysis; 4) Ru-based bimetallic oxides, the synergistic effect of metal elements and nonmetal O to tune the electronic structure of Ru-based catalysts; 5) size engineering strategies, reducing the size of Ru-based materials highly enhances the metal atom utilization and specific catalytic activity; 6) heterostructure engineering strategies, charge redistribution at the heterointerface leads to favorable electronic structure and boosted catalytic capability.

2.1. Surface Structure Engineering Strategies

The Ru surface structures, including crystal phase and morphology, have a vital influence on the structural and catalytic properties.[35] The rearrangements of surface Ru atom induced by the crystal phase structures affect the electronic structure and thus their catalytic capability. Ru nanocrystals generally have two crystal structures, namely, hexagonal close-packed (hcp) and face-centered cubic (fcc).[30] Metallic Ru thermodynamically favors the hcp structure, while the fcc structure is metastable. However, the Ru—Ru bond strength in the fcc structure is always greater than that in the hcp structure.[36–38] Due to their different atomic arrangements, the fcc and hcp phase Ru nanocrystals possess different catalytic activities, respectively. A simple solvothermal method can be used to obtain the Ru nanosheets with hcp phase. The characterization results demonstrated the presence of the (100) and adjacent (002) facets in hcp Ru nanocrystals. Density function theory (DFT) calculations indicate the hollow sites in the (001) fact of the hcp are responsible for the smaller Gibbs free energy of hydrogen (ΔG_{H^*}) and boosted HER performance (**Figure 2**a,b).[39] Nevertheless, it is reported that fcc-phase Ru catalysts exhibited superior catalytic performance to those of hcp-phase Ru catalysts.[40,41] For instance, it is found that the Ru fcc (111) in $Ru/C_3N_4/C$ is active to lower the water dissociation energy barrier and weaken the H bonding for HER in 0.1 M KOH solution, delivering the overpotential of about 40 mV lower than that of Ru hcp (Figure 2c,d).[42] The fcc-Ru was also revealed to be more favorable for HOR. The designed unconventional fcc-Ru/C with twinning and stacking fault structures exhibited superior HOR activity than that of hcp-Ru/C with the same particle size due to the stronger OH* binding ability (Figure 2e,f).[43] In addition to being composed of pure hcp or fcc phases, Ru nanocrystals can also be prepared with mixed fcc and hcp phase structures, which promote HER catalytic activity under their synergistic effect.[44]

The morphology of Ru nanocrystals can induce the exposure of specific facet and alter the electrocatalytic process. The fcc-structured octahedrons, truncated cubes, and nanoparticles have been prepared, and fcc-Ru octahedra exhibited the lowest overpotential for OER (η_{10} = 168 mV) compared to truncated cubes (η_{10} = 189 mV) and nanoparticles (η_{10} = 197 mV) in 0.5 M H_2SO_4 solution. This is due to the fact that the truncated cubes are covered by {100} planes, whereas fcc-Ru octahedra are surrounded by {111} planes. The {111} facets more effectively lower the reaction energy barrier, thereby promoting the OER reaction.[45] In addition, the specific crystal face exposed by the design of special morphology also helps to inhibit the dissolution of Ru atoms on the surface and increase the stability of the

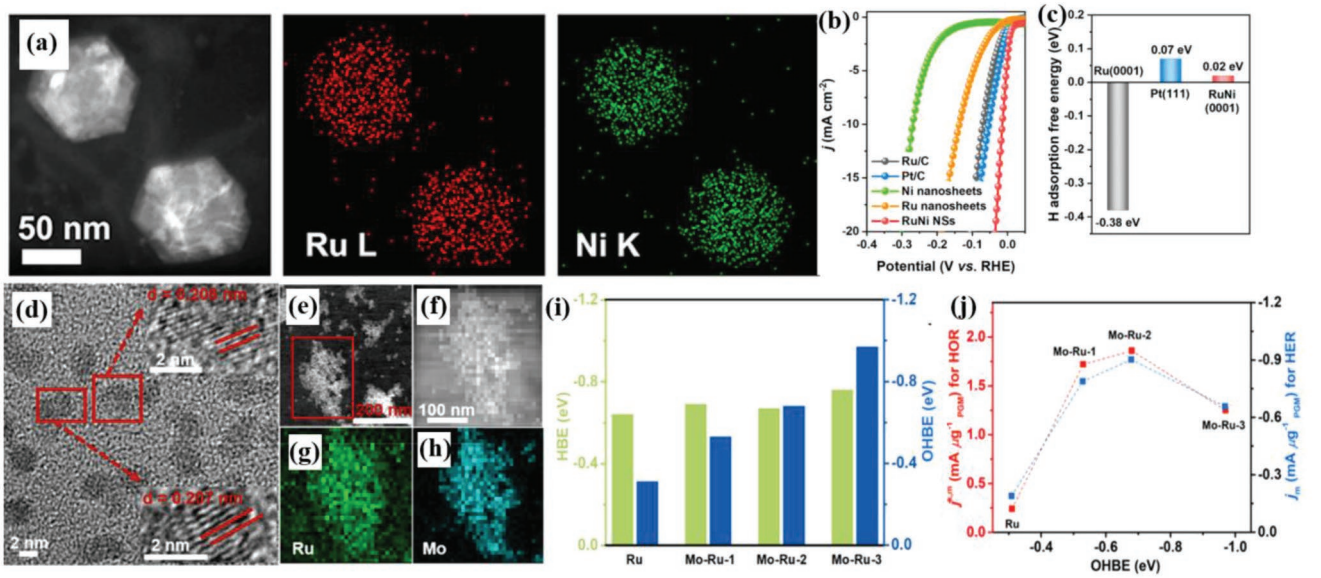

Figure 3. a) HAADF-STEM and corresponding energy dispersive spectroscopy (EDS) elemental mapping images of RuNi NSs. b) HER polarization curves of RuNi NSs and comparative samples. c) Free energies of H adsorption on Ru, Pt, and RuNi surfaces. Reproduced with permission.[59] Copyright 2019, Elsevier. d) TEM, e–h) HAADF-STEM images, and EDS elemental mapping of Mo-Ru-2. i) HBEs and OHBEs and j) $j_{k,m}$ of the alkaline HOR and j_m of the alkaline HER vs OHBE values of Ru, Mo-Ru-1, Mo-Ru-2, and Mo-Ru-3. Reproduced with permission.[61] Copyright 2022, American Chemical Society.

catalyst. Ru-branched nanoparticles with hcp crystal phase structure expose more {0001}, {10–10}, and {10–11} low-index crystal planes than polycrystalline Ru nanoparticles. The low-index surface has fewer high-energy defect sites, which provides a slow Ru dissolution rate. The branched nanoparticles still maintained high OER catalytic activity within 4 h, while the polycrystalline nanoparticles had a large amount of Ru dissolution within 1 min, leading to catalyst deactivation (Figure 2g,h).[46]

2.2. Metal Element Engineering Strategies

Alloying is an effective strategy to tune the intrinsic catalytic activity of the metal hosts.[47] Due to the different atomic radius and electronegativity, the electronic structure of Ru can be easily adjusted when incorporating other metal elements into the lattice, and thus promote the electrocatalytic activity. Moreover, the incorporated metal element can also act as additional active sites to synergistically accelerate the catalytic reaction. Due to the excellent corrosion resistance and high catalytic activity of noble metals (such as Pt, Ir, Pd, and Au), alloying with Ru will significantly improve the corresponding intrinsic activity. PtRu is the most studied alloyed material, which has been widely used as electrocatalysts for HOR, HER, etc.[48–51] Ru atoms possess stronger oxidophilicity than Pt atoms. Therefore, a bifunctional mechanism can be found in PtRu alloys, which arises from the synergistic effect of Pt and Ru. In terms of HOR, Ru acts as an active site to adsorb OH* to accelerate the generation of H_2O.[52] Moreover, the electronic effect between Pt and Ru weakens the adsorption of H* by PtRu.[53] Alloying combined with morphology design can further increase the catalytic activity. RuIr nanosized-coral (RuIr-NC) with a special coral-like structure exhibited superior OER activity and stability compared to their spherical counterpart (RuIr-NS). The anisotropic RuIr-NC consists of a solid solution of hcp phase with exposed extended {0001} planes. The exposed {0001} faces with the lowest surface energy effectively inhibit the oxidation of both Ir and Ru in RuIr-NC, enabling long-term stable properties during acid chronopotentiometry testing for up to 120 h.[54]

Alloying Ru with the abundant transition metals (Fe, Co, Ni, Cu, etc.) can not only modify the electronic structure of Ru to enhance or maintain the catalytic ability, but also highly reduce the corresponding cost.[55–58] For example, RuNi alloys (RuNi NSs) stacked with multilayer hexagonal nanosheets were synthesized using a one-pot hot solvent method.[59] Ru and Ni elements were uniformly distributed on the nanosheets (**Figure 3**a). When RuNi NSs were used as electrocatalysts for alkaline HER, a current density of 10 mA cm^{-2} can be achieved at the overpotential of 15 mV, which is significantly better than those of single metal Ru NSs (η_{10} = 134 mV) and Ni NSs (η_{10} = 248 mV)-based catalysts (Figure 3b). The DFT results have revealed that the introduction of Ni leads to the optimized H adsorption free energy on RuNi NSs, which promotes H adsorption and desorption processes (Figure 3c). Moreover, it is worth mentioning that transition metal cations with unpaired d electrons or empty d orbitals can activate reaction intermediates to promote the catalytic reactions after alloying with Ru.[60] For example, the transition metal Mo with unpaired d electrons has been incorporated into Ru NPs for basic HOR/HER reaction (Figure 3d–h). DFT calculations showed that the OH* binding energy on Mo-Ru/C exhibited an ascending trend with increasing Mo content (Figure 3i). Figure 3j shows a volcano-type relationship between the HOR/HER activity and hydroxide binding energy (OHBE) value of Mo-Ru in alkaline media, and Mo-Ru-2 with moderate OHBE strength is responsible to the enhanced HOR/HER activity.[61]

2.3. Nonmetal Element Engineering Strategies

Nonmetallic heteroatoms (O, P, B, S, N, etc.) possess high electronegativity, and the local coordination environment of Ru can be optimized by forming Ru-heteroatom bonds, resulting in a larger electron transfer from Ru to these heteroatoms. Thus, the electron density and d-band center of the active metal site are carefully altered, which facilitates the adsorption of reactants and intermediates.[62,63]

The incorporation of O atoms to Ru crystal structure forming RuO_2 has been considered promising OER catalysts due to the relatively higher activity. Ru is coordinated with five O atoms in RuO_2 (110) facet to form an unsaturated site (Ru_{cus}), which is the adsorption site for water molecules in the acidic OER process to preferentially generate *OOH through successive deprotonation.[32,64] In addition, high-index crystal planes usually have more steps, kinks, etc., with high surface energies and active sites containing atoms with low coordination numbers. Exposing the high-index surface is conducive to the adsorption of active intermediates to further enhance the catalytic activity of RuO_2.[65–67] Except for the crystallized structure, the RuO_2 with the amorphous phase possesses randomly arranged atom distribution, which not only produces a large number of unsaturated sites and defects, but also leads to a certain self-regulation and antidisturbance ability in the structure, boosting the corresponding catalytic activity and stability.[68,69] For example, RuO_2 with ordered crystalline and disordered amorphous phases coexist (a/c-RuO_2) has been prepared. The amorphous structure improves the adsorption of reactants and lowers the OER reaction energy barrier of the rate-determining step (RDS). In addition, the flexible structural properties of a/c-RuO_2 inhibit the dissolution of Ru due to excessive oxidation and maintain stability. The η_{10} of a/c-RuO_2 in electrolytes at pH 0, 7, and 14 are 220, 287, and 235 mV, respectively, which are significantly lower than that of commercial RuO_2 (322, 470, and 312 mV, respectively).[70]

Similar to O element, phosphorus (P) is another promising nonmetal element to be incorporated to engineer the structural and catalytic properties of Ru-based catalysts. P as electron acceptors can induce the electrons to transfer from Ru to P when forming Ru—P bonds, highly reducing the electronegativity of Ru and thus enhancing the corresponding HER catalytic activity.[71,72] For example, P—Ru NPs were obtained with uniform distribution of Ru and P elements, suggesting P is successfully incorporated into Ru NPs (**Figure 4**a). P-Ru/C exhibited superior HOR/HER mass activity (MA) compared to the undoped Ru/C, ascribing to the modulated electronic structure and negatively shifted d-band center of Ru atoms induced by P incorporation, which highly enhanced the H_2 desorption ability in the HER process and changed the RDS from water formation to water desorption step in the HOR process (Figure 4b,c).[73] The light element B with a small atomic radius has a moderate electronegativity between metals and nonmetals.[74] When B is introduced into the Ru atomic structure, it can also induce the electrons redistribution, forming a strong ligand effect of sp-d orbital hybridization between B and Ru atoms, which makes the d-band center of RuB move down (Figure 4d,e). This results in an extremely low ΔG_{H^*} value (close to zero) and overpotential (η_{10} = 22 mV) for RuB, which is significantly superior to that of metallic Ru ($\Delta G_{H^*} \approx -0.6$ eV, $\eta_{10} \approx 110$ mV).[75]

2.4. Ru-Based Bimetal Oxides

As discussed above, incorporating O atoms to Ru crystal structure forming RuO_2 is a promising strategy to achieve boosted catalytic activity. Further engineering RuO_2 by metal element forming bimetallic oxides may further tune the electronic structure and synergistically accelerate the catalytic reactions. The incorporated additional metal element to RuO_2 can efficiently balance the catalytic activity and stability to compensate the drawbacks of RuO_2 (poor stability) in the catalytic process.[76,77] In addition, the additional second metal element can also directly serve as active sites, opening up new horizons for the electrocatalytic applications of Ru-based bimetallic oxides. Currently, the most investigated second metal element for RuO_2 are noble metals (Ir, Pt, etc.) and nonprecious metals (Cu, Fe, Co, Ni, Mn, etc.).

IrO_2 is one of the most promising electrocatalysts for OER with excellent performance. Metal Ir (0.077 nm) shares a similar atomic radius to that of Ru (0.076 nm).[78,79] Therefore, when metal Ir is introduced into Ru oxide, a bimetallic oxide solid solution phase can be formed, in which the Ru and Ir elements are uniformly distributed. The incorporated Ir can significantly enhance the corrosion resistance of RuO_2 in electrocatalytic conditions.[35] For instance, the $IrRuO_x$ solid solution nanoparticles supported by TiO_2 ($IrRuO_x/TiO_2$) have been prepared by impregnation and thermal oxidation method. The achieved $IrRuO_x/TiO_2$ delivered 1.33 times higher mass activity compared to that of mechanically mixed unsupported IrO_2-RuO_2. Moreover, the presence of Ir in $IrRuO_x/TiO_2$ effectively avoided the irreversible reaction to generate the hydrated Ru^{4+} and Ru^{6+}, which stabilized the intermediate RuO_4 and inhibited the Ru dissolution. The $IrRuO_x/TiO_2$ achieved excellent stability with only 7% decay after 100 CV (cyclic voltammetry) cycles, whereas the mechanically mixed IrO_2-RuO_2 were decreased by 15%.[80] Moreover, $Ir_xRu_{1-x}O_y$ bimetallic oxides with nanofibrous structure showed superior HER electrocatalytic activity over RuO_y after cathodic polarization in 1 M NaOH solution. The Tafel slopes of $Ir_xRu_{1-x}O_y$ and RuO_y are 31.5 and 47.8 mV dec^{-1}, respectively. Through sustained cathodic polarization, the surface Ru and Ir oxides of $Ir_xRu_{1-x}O_y$ are partially reduced to metallic Ru and Ir, thus showing the optimum H* adsorption energy.[81]

The introduction of transition metals with high conductivity into RuO_2 can also adjust the electronic structure and improve the intrinsic activity, thus increasing the active sites and optimizing the Gibbs free energy. For example, the as-prepared hollow polyhedral Cu-doped RuO_2 (Cu/RuO_2) OER electrocatalysts exhibited accumulated electrons on Ru sites due to the replacement of Ru by Cu atoms generating O vacancies. This results in unsaturated coordinated Ru active atoms on the surface, leading the O p-band center of Cu/RuO_2 closer to the Fermi level (shifting from –4.52 to –3.97 eV), thereby increasing the charge transfer and OER kinetics.[82] Moreover, Fe, Co, or Ni transition metals with empty 3d orbitals can also engineer RuO_2 to achieve the suitable d-band center and optimized adsorption energy of OH* or H* active intermediates. For example, $MRuO_2$ (M = Fe, Co, and Ni) bimetallic oxides were prepared by a combination of a simple wet chemical method and thermal annealing in air. $MRuO_2$ exhibited excellent OER

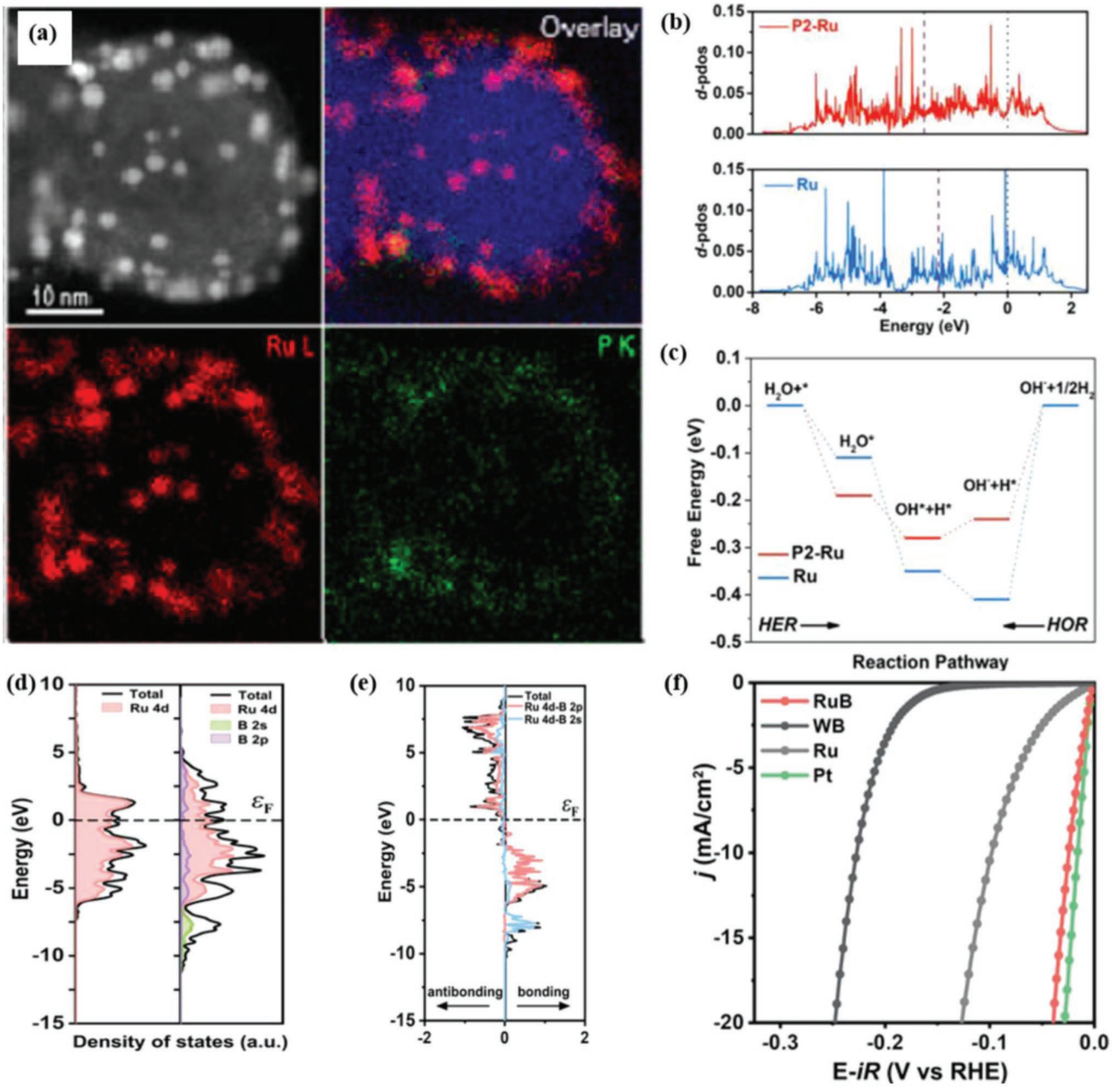

Figure 4. a) Energy dispersive X-ray analysis (EDX) elemental mapping of Ru and P in P-Ru/C. b) Partial density of states (PDOS) and c) reaction pathways for alkaline HER and HOR of P2-Ru and pure Ru. Reproduced with permission.[73] Copyright 2020, American Chemical Society. d) DOS and PDOS of Ru (0001) and RuB (001) planes. e) The crystal orbital Hamiltonian population (COHP) of Ru—B bonds in RuB. f) Polarization curves of HER in acidic solution. Reproduced with permission.[75] Copyright 2020, Wiley-VCH.

and HER activity in electrolytes with a wide range of pH values (0.05/0.5 M H_2SO_4, 0.1/1 M KOH). The introduction of Fe, Co, and Ni transition metals made the overpotentials of the Ru-based bimetallic metal oxides show an inverted volcano plot relationship with the active intermediates of OER (OH*) and HER (H*), where Co-RuO_2 and Ni-RuO_2 are located at the lowest points for OER and HER, respectively, showing the best catalytic activities.[83]

In addition to the aforementioned Ru-based bimetallic metal oxides, pyrochlore-type ($A_2B_2O_7$) Ru-based oxides also possess unique physicochemical properties and stable structures for electrocatalytic reactions. Pb^{2+}, Bi^{3+}, and Y^{3+} are often used as the A-site cations of pyrochlore oxides, which effectively changes the center energy of the overlap of Ru 4d with O 2p orbitals.[84–86] $Y_2Ru_2O_{7-\delta}$ prepared by the sol–gel method has delivered a low onset potential of 1.42 V vs reversible hydrogen electrode (RHE) in 0.1 M $HClO_4$ media, which is much lower than that of RuO_2 (≈ 1.47 V). Furthermore, $Y_2Ru_2O_{7-\delta}$ showed much enhanced stability with no obvious decay after 10 000 CV cycles, whereas the undoped RuO_2 was

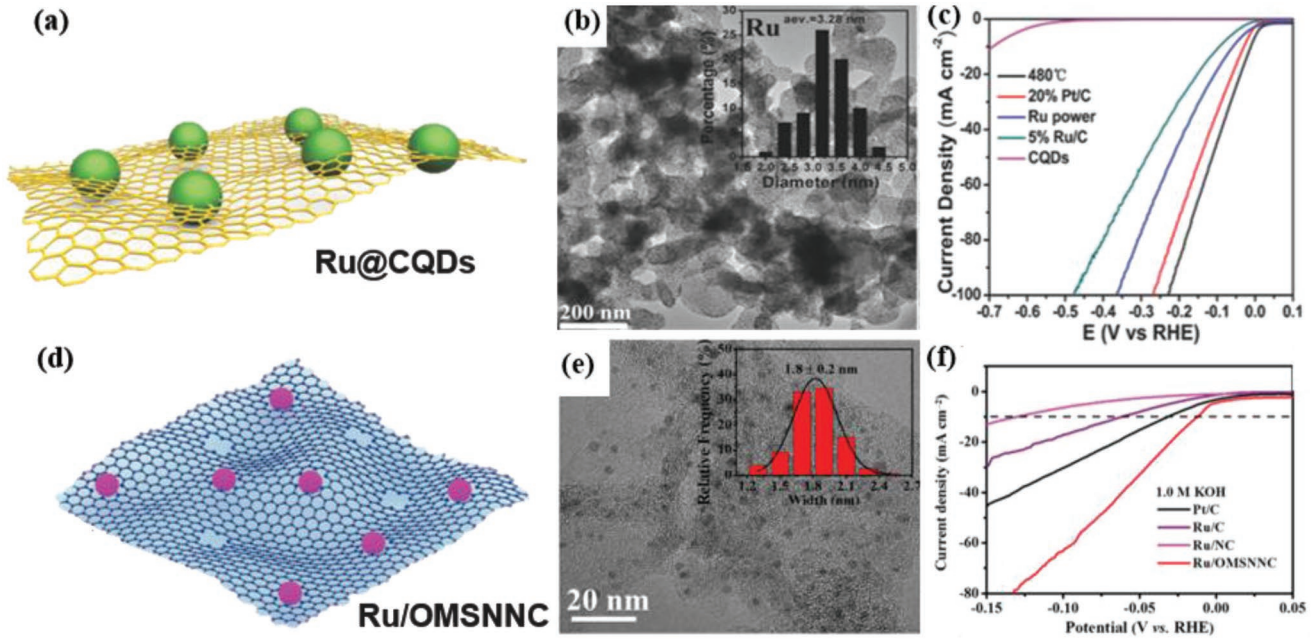

Figure 5. a) Schematic diagram of the structure of Ru NPs dispersed on CQD. b) TEM image (inset: corresponding particle size distribution of Ru NPs). c) HER polarization curves of Ru@CQDs (480 °C) and other samples in 1 M KOH solution. Reproduced with permission.[88] Copyright 2018, Wiley-VCH. d) Schematic diagram of the structure of Ru nanoclusters dispersed on OMSNNC. e) TEM image (inset: corresponding particle size distribution of Ru nanoclusters). f) HER polarization curves of Ru/OMSNNC, Ru/NC, Ru/C, and Pt/C in 1 M KOH solution. Reproduced with permission.[91] Copyright 2021, Wiley-VCH.

almost inactivated after cycling. The boosted OER catalytic performance is mainly attributed to the introduction of Y^{3+} cations at the A-site, which enables Ru in $Y_2Ru_2O_{7-\delta}$ to have a lower oxidation state and significantly different Ru—Ru bonds in RuO_2, promoting the adsorption of active intermediates of HOO*. In addition, the presence of Y^{3+} metal ions lowers the center of the overlapping energy band of Ru 4d and O 2p orbital, showing more stable Ru—O bonding, thereby enhancing the OER stability of $Y_2Ru_2O_{7-\delta}$.[87]

2.5. Size Engineering Strategies

With the leap forward in surface science, researchers find that the surface of small-sized Ru nanoparticles is rich with unsaturated atoms and defects compared to bulk Ru, exposing more active sites to boost the catalytic activity. In addition, the unique electronic effects on small-sized Ru nanoparticles (e.g., 3.28 nm) and carbon substrates accelerate charge transfer and facilitate H_2O adsorption/dissociation for alkaline HER (**Figure 5**a–c).[88] Further downsizing nanoparticles to nanoclusters (NCs) composed of a few or hundreds of atoms (average size about 2 nm) exhibits fascinating electrocatalytic performance with strong quantum size effects.[89,90] The as-prepared ultrafine Ru clusters supported on N-doped nano-ordered porous carbon frameworks (Ru/OMSNNCs) exhibited outstanding HER performance, benefiting from the nanocrystal-rich active surfaces and interconnected porous supports (Figure 5d–f).[91]

It is worth mentioning that a large number of active sites inside Ru nanoparticles or clusters are inaccessible in electrocatalysis. Therefore, only a small fraction of Ru atoms on the surface participates in the electrocatalytic reaction, which loses a large number of active atoms. Single-atom catalysts (SACs) maximize the usage of all active atoms and enhance mass activity.[92–94] The high surface energy of Ru single atoms requires to be stabilized on a suitable supporting substrate to prevent agglomeration during the preparation and catalytic conditions. The heteroatom-doped carbon supports with large specific surface area and electrical conductivity are promising candidates to firmly anchor Ru single atoms for electrocatalysis. As shown in **Figure 6**a,b, Ru single atoms (SAs) are dispersed on N-doped graphene oxide (Ru-N/G) and stabilized by surrounding N atoms. The coordination of N with Ru high-valent Ru-oxo species to form Ru-oxo-N_4 structure is the source of the activation performance of acidic ORR (Figure 6c).[28] In addition, Ru-Pt bimetallic dimers on carbon substrate also show excellent catalytic activity. The Pt atoms strongly affect the electronic structure of Ru atoms, making the Ru-Pt dimers transform from metal to semiconductor with increasing H adsorption, which reduces the ΔG_{H^*} of the dimers (Figure 6d,e).[95]

In addition to carbon substrates, noncarbon substrates, such as alloys, metal oxides, metal hydroxides, metal nitrides, etc., are also good carriers for supporting Ru SAs. The Ru SAs can be stabilized by the metal or nonmetal element in these noncarbon supports. HER catalyst of $NiRu_{0.13}$-BDC with Ru monodispersed in Ni-based metal-organic framework (Ni-BDC) has been prepared by ion exchange (Figure 6f).[96] Ru SAs directly interacts with Ni atoms in the support, which causes charge accumulation around Ru and charge depletion around Ni, significantly affecting the adsorption strength of $NiRu_{0.13}$-BDC for H_2O and H* intermediates (Figure 6g). In addition, the Ru SAs were stabilized by O atoms forming a Ru-O-Co/Fe ligand

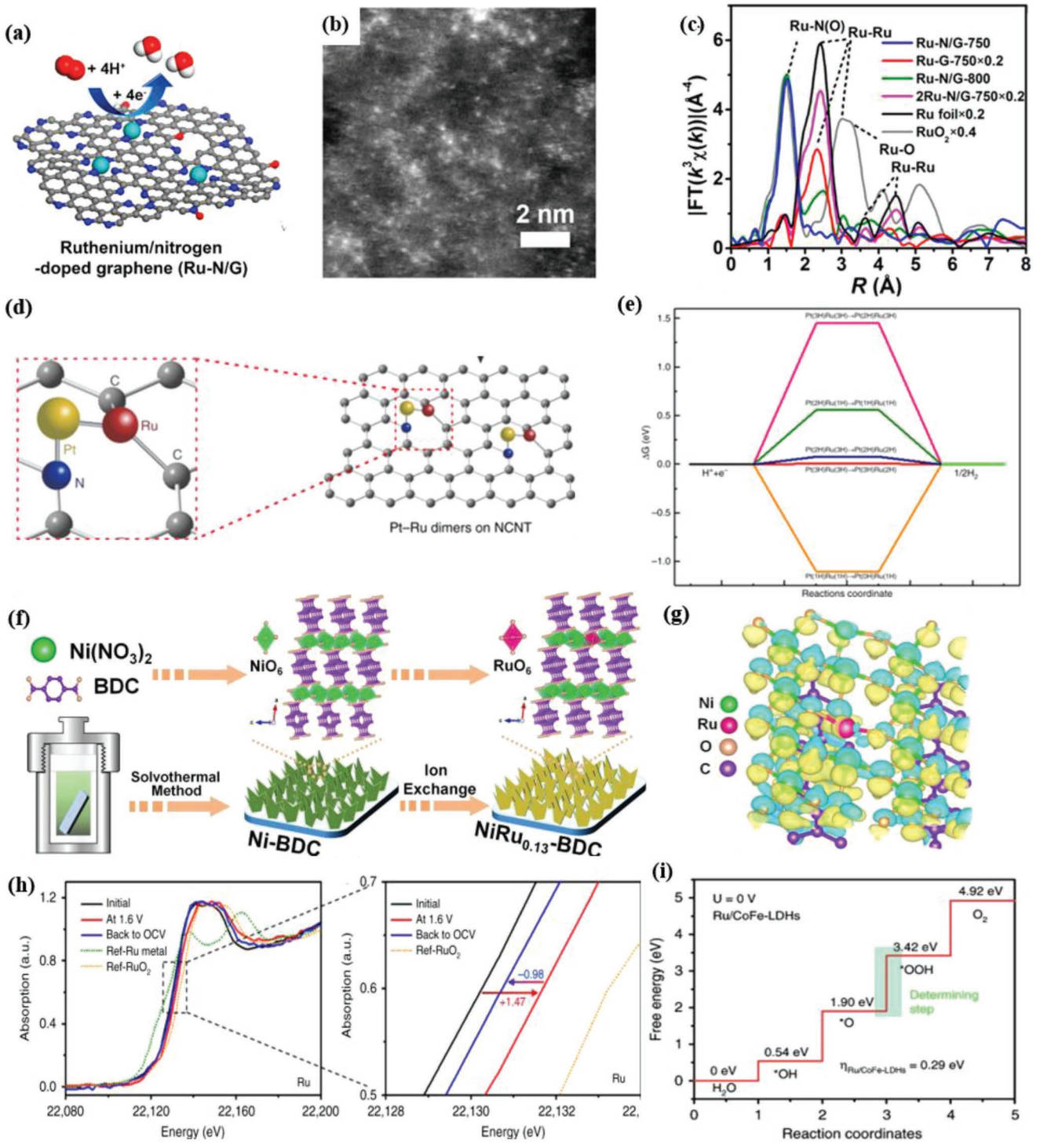

Figure 6. a,b) Structural simulation and HAADF-STEM of Ru-N/G SACs. c) Fourier transform magnitudes of the experimental Ru K-edge extended X-ray absorption fine structure (EXAFS) spectra of the Ru-N/G and other comparative samples. Reproduced with permission.[28] Copyright 2017, American Chemical Society. d) Structural simulation of Pt-Ru dimer dispersed on NCNT. e) ΔG_{H^*} plots for different H coverages. Reproduced with permission.[95] Copyright 2019, Nature Publishing Group. f) Schematic illustration of the synthesis of $NiRu_{0.13}$-BDC by ion-exchange method. g) The simulated charge difference between $NiRu_{0.13}$-BDC and Ni-BDC. Yellow represents charge accumulation and blue represents charge depletion. Reproduced with permission.[96] Copyright 2021, Nature Publishing Group. h) In situ X-ray absorption near edge structure (XANES) of Ru K-edge under OER electrochemical conditions. i) Gibbs free energy diagram during OER process on Ru/CoFe-LDHs. Reproduced with permission.[97] Copyright 2019, Nature Publishing Group.

structure in Ru SAs/CoFe LDH. Electron transfer from Co/Fe to Ru through O bridge maintains Ru with an oxidation state below +4 during OER process and promotes the formation of OOH* intermediate, ensuring the OER activity and stability (Figure 6h,i).[97]

2.6. Heterostructure Engineering Strategies

Heterostructures composed of Ru species and other metals, metal oxides, metal phosphides, metal sulfides, etc., are also effective to improve the catalytic activity of Ru-based electrocatalysts. Electron transfer often occurs at the heterointerface of different components, resulting in the charge redistribution and favorable adsorption of reactive intermediates. For example, the Ru_2P@Ru/CNT heterostructure prepared by the microwave method has an HER overpotential of 23 mV in 1.0 M KOH, which is significantly smaller than those of Ru_2P/CNT (29 mV) and Ru/CNT (46 mV). The heterojunction formed between Ru and Ru_2P not only increases the electrochemically active specific surface area of Ru_2P@Ru/CNT, but also enables electron transfer from Ru to P atoms, facilitating the HER process.[98] In addition, the mutual stretching/compression at the interfaces in the core–shell heterostructure can also tune the electronic structure of Ru-based catalysts. For example, a Pt shell of three to six atomic layers covered the hcp and fcc phase Ru nanosheets, respectively. Due to the stronger strain effect and surface energy of the fcc phase Ru, the characteristic peaks of X-ray photoelectron spectroscopy (XPS) of shell Pt 4*f* are shifted to a more positive direction, which promotes the methanol oxidation reaction.[99]

3. Electronic Modulation Effect

Electrocatalytic reactions are heterogenous processes dominated by the surface of solid catalysts, which usually involve multiple reaction intermediates. Therefore, the binding ability between the intermediates and active sites plays a decisive role for catalytic activity. Tuning the electronic structure of the catalysts is considered to be the most straightforward way to alter the adsorption/desorption behavior of intermediates, and thereby the catalytic performance. The above-summarized engineering strategies can efficiently alter the electronic structure of Ru-based nanomaterials through composition optimization/doping and phase/interface adjustment. Thorough investigation of the induced effects is beneficial to understand the relationship between the atomic structure of Ru-based catalysts and the corresponding catalytic activity. We will classify the induced effects into intramolecular electronic modulation effect and intermolecular electronic modulation effect in Ru-based nanocatalysts. Intramolecular electronic modulation effect refers to the occurrence of metal/nonmetal doping and surface structure optimization, whereas intermolecular electronic modulation effect refers to the interaction between different components in the heterostructure or between active molecules and supports. Both of intramolecular and intermolecular electronic modulation effects can induce the charge redistribution and influence the catalytic capability. First, the intramolecular electron modulation effect of heteroatom doping promotes the spontaneous migration of electrons to the atoms with stronger electronegativity, resulting in charge redistribution. The different surface structures of nanocatalysts usually generate atoms with different coordination numbers (CN), which change the d-band center of the catalyst and thus affect the adsorption capacity of intermediates. Second, the intermolecular electronic modulation effect is the charge transfer between distinct interfaces, such as hetero-interfaces and active molecule-support interfaces, prompting the charge redistribution on the interface. Intramolecular and intermolecular electronic modulation effects not only affect the physical properties of materials such as electrical conductivity, but also affect the adsorption capacity of intermediates, which is an important basis for improving catalytic activity. To fully exploit the potential of Ru-based nanomaterials, researchers often use a combination of modification strategies to construct suitable electronic mechanisms. In the following section, we will discuss the resulted electronic modulation effects from both intramolecular and intermolecular aspects for Ru-based materials.

3.1. Intramolecular Electronic Modulation Effect

The intramolecular electron modulation effect is mainly caused by metal or nonmetal element incorporation. The different ionic radius and electronegativities between Ru and the incorporated heteroatoms can inevitably induce the electron transfer, resulting in the charge redistribution around Ru atoms, thereby boosting the catalytic activity. Nonmetallic heteroatoms with smaller atomic radius and larger electronegativity can attract electrons, making the Ru atoms with an electron-deficient structure or phase distortion. This effectively tunes the electronic structure and changes the d-band center of the catalysts and thus affecting the catalytic activity. For instance, the pyrite-type RuS_2 nanomaterials with the S element resulted in intermittent lattice fringes, indicating the formation of disordered structures, which increases the electrochemical surface area and HER, OER catalytic activity.[100]

Incorporating metal element can also modulate the electronic structure of Ru-based catalyst, and meanwhile it may also lead to additional active sites.[101] Ru possesses a strong binding ability to H, making it unfavorable for H desorption in HER, whereas Cu shows a weak binding ability to H, making it difficult to adsorb H. When Ru and Cu are alloyed, the formed electronic modulation effect can efficiently promote the HER process.[56] Specifically, characterization results indicated the electrons transferred from Cu to Ru atoms after alloying (**Figure 7**a–d,g). DFT calculations further verified that the electronic modulation effect makes both the water dissociation energy barrier and H* adsorption free energy of Ru and Cu sites in the alloy smaller than those of the counterparts with a single Cu or Ru metal (Figure 7e,f). In addition, Nanba et al. also found that the coordination number of surface atoms in hcp and fcc phases with different morphologies significantly affects the d-band center of Ru NPs by DFT calculations. The surface of icosahedral fcc Ru NPs has only {111} crystal planes with the largest average coordination number, which makes its d-band center smaller than that of hcp Ru NPs and truncates

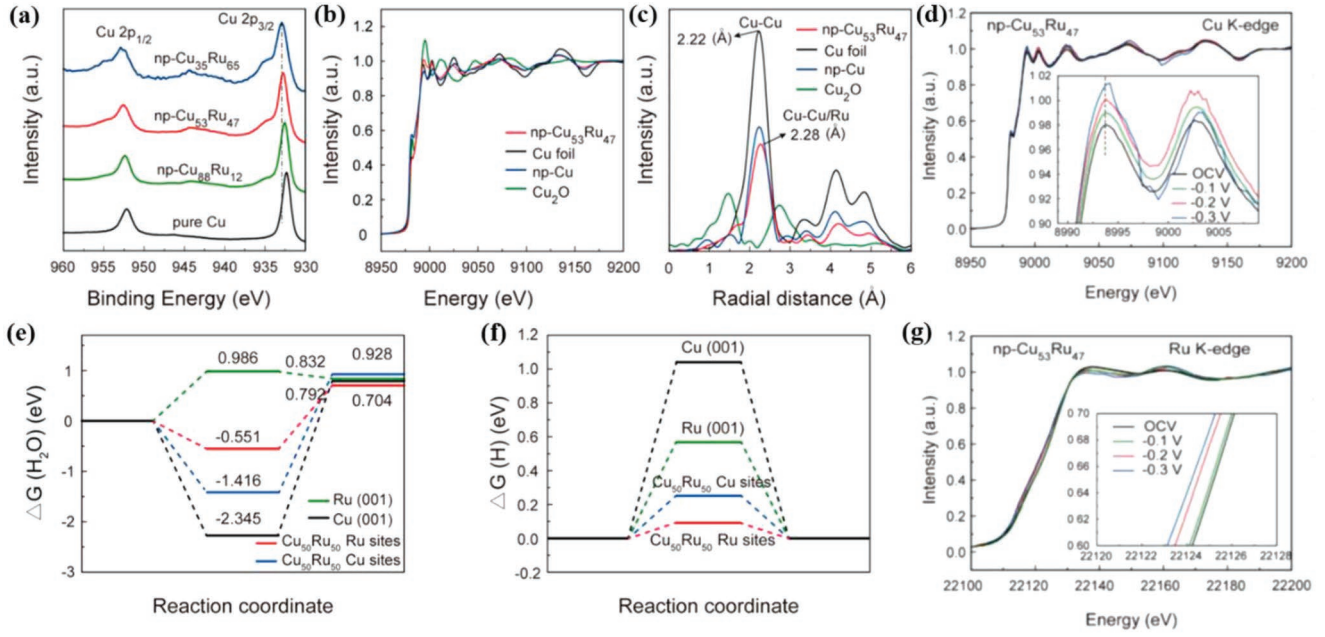

Figure 7. a) XPS spectra of Cu 2p with different Cu/Ru atomic ratios. b) Normalized XANES and c) FT-EXAFS for the Cu K-edge. Operando XANES spectra during HER process at d) the Cu K edge and g) Ru K-edge of np-$Cu_{53}Ru_{47}$ at different applied voltages. e) Free energy diagram of the adsorption step of H_2O on Ru and Cu sites in $Cu_{50}Ru_{50}$ alloy. f) H adsorption free energy diagram. Reproduced with permission.[56] Copyright 2020, American Chemical Society.

octahedral fcc Ru NPs about 0.2–0.4 eV. And the icosahedral fcc Ru NPs have negative twin boundary energy, which further stabilizes the nanoparticle structure. The obtained conclusions provide a theoretical basis for the future surface structure design of Ru nanocatalysts from electronic structure and stability.[102]

3.2. Intermolecular Electronic Modulation Effect

The intermolecular electron modulation effect is induced by the interaction among core–shell, heterostructure, or catalyst-support interface to tune the electron distribution of Ru-based catalysts, thereby optimizing the adsorption energy of reactants/intermediates.[103,104] Fabrication of ultrathin shells at the atomic scale can change the chemical properties and surface electronic structures of core–shell structure materials, so that the catalytic activity exhibits a dependence on the thickness of the shell. For example, PdO@RuO_2 hexagonal nanosheets with shell thicknesses of two, four, and six atomic layers were obtained after the thermal oxidation of Pd@Ru NSs (**Figure 8**a,b).[105] The PdO@RuO_2 NSs with two and six overlayers shifted the d-band center up due to their strong binding ability to O*, while the d-band center with four atomic layers shifted down, showing weakened O* binding ability, which promoted the formation of OOH* key intermediates in the acidic OER process (Figure 8c). In addition, the core–shell structure may result in a high-strength strain at the core/shell interface, leading to superior catalytic activity than conventional strain-free materials.[106] The negative shift of the Pt–Ru and Pt–Pt peaks in Ru@Pt icosahedral core–shell structure indicates the presence of compressive strain in the Pt shell (Figure 8d,e), making Ru@Pt favorable to the OH* and H* adsorption in the HER process, thus enhancing the alkaline HER catalytic activity.[107]

Electrons spontaneously transfer between different structures at the interface of heterostructure promoting the adsorption capability of intermediates on the catalyst surface.[108,109] For example, Ru–RuO_2 Mott–Schottky (MS) heterojunctions consist of typically closely contacted twinned nanocrystals of Ru and RuO_2 (Figure 8f,g). The strong interaction between the heterostructure of Ru and RuO_2 enables electron transfer from Ru to RuO_2, which leads to the up-shifted d-band center of Ru–RuO_2, thereby facilitating the adsorption/desorption of the intermediates in OER and HER processes (Figure 8h,i).[110]

The interaction of Ru with the carrier plays an important role in optimizing the local geometric and electronic structure on the Ru active site, which is caused by their different Fermi levels and work functions. Highly ordered carbon materials can be used as models to study the electronic modulation effect between Ru and supports. The introduction of highly electronegative heteroatoms (N, P, S) and/or defects into carbon materials will increase the loading and dispersion of Ru atoms, thereby enabling charge redistribution to facilitate the chemisorption. For example, a triazine ring (C_3N_3)-doped carbon support (triNC) with high local nitrogen density increases the work function of the carbon support, which leads to the highest electron loss of Ru atoms (Figure 8j–n). The charge redistribution from Ru to triNC enables Ru/triNC to exhibit strong hydrolysis ability and moderate H adsorption strength (Figure 8o,p).[111] In addition, noncarbon supports such as metal-based oxides, carbides, phosphides, and nitrides have more complex electronic structures. The 2D MXenes not only have high specific surface area and excellent electrical conductivity, but also present abundant single vacancies or vacancy clusters.[90] Ru single atoms on

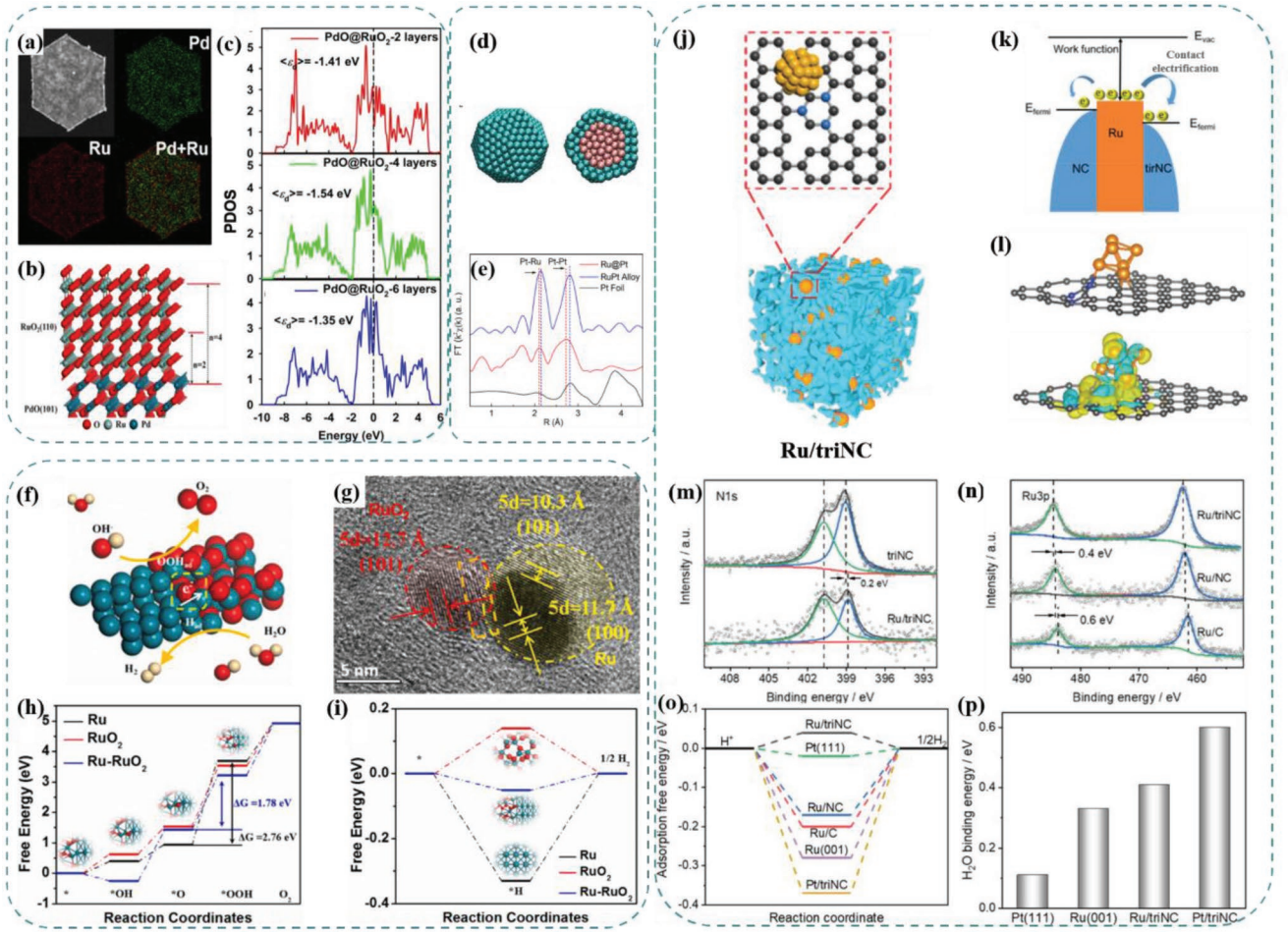

Figure 8. a) HAADF-STEM and corresponding EDS elemental mapping images of Pd@Ru NS. b) Schematic illustration of the surface structure of PdO@RuO_2 hexagonal nanosheets. c) PDOS of 4d band of top layer Ru atoms PdO@RuO_2-2layers, PdO@RuO_2-4layers, and PdO@RuO_2-6layers with respect to the Fermi level. Reproduced with permission.[105] Copyright 2019, American Chemical Society. d) Atomic structural model of the Ru@Pt icosahedron. e) Pt L_{III}-edge R-space EXAFS spectrum. Reproduced with permission.[107] Copyright 2018, American Chemical Society. f) Schematic diagram of the structure and g) HR-TEM image of Ru-RuO_2@NPC. Free energy diagrams of h) OER and i) HER. Reproduced with permission.[110] Copyright 2021, Elsevier. j) Structure diagram of Ru/triNC. k) Illustration of contact electrification in Ru/triNC and Ru/NC. l) Differential charge density of Ru/triNC. Gray, blue, and orange spheres represent C, N, and Ru atoms, respectively. XPS spectra of m) N 1s and n) Ru 3p. Changes in the binding energies of o) H_2 and p) H_2O in Pt/triNC. Reproduced with permission.[111] Copyright 2020, Wiley-VCH.

Mo_2CT_X MXene nanosheets (SA Ru-Mo_2CT_X) have been prepared and the large number of vacancies and functional groups such as O^{2-} and OH^- in Mo_2CT_X can efficiently adsorb Ru(III), leading to high loading of 1.41 wt%. The Ru atoms are stabilized by the surrounding O atoms and the formed Ru—O bonds elevate the Ru d-band center, which improves adsorption of intermediates and lowers the reaction energy barrier.[112]

4. Electrocatalytic Performance of Ru-Based Nanomaterials

The energy depletion, environmental pollution, and global warming stimulate the development of sustainable and clean energy conversion technologies to achieve carbon neutrality. Electrocatalytic reactions play a central role in energy conversion devices, especially those involving H_2 or O_2 conversion-related electrocatalytic reactions in sustainable processes for water electrolysis devices and fuel cells. Metallic Ru has suitable H* adsorption energy and OH* binding capacity, which is suitable for the electrocatalytic reaction of H_2–O_2 conversion.[113] In order to further increase the catalytic activity, the structure modification strategies of Ru-based nanomaterials with more exposed active sites and modulated electronic structure are essential. For instance, element doping and heterostructure can result in efficient charge redistribution, altering the electronic structure of Ru and boosting the catalytic ability. Downsizing bulk Ru to single atom scale generates unsaturated coordination, maximizing atom utilization, and appealing for the adsorption of reactants/intermediates. The engineering strategies enable Ru-based catalysts to achieve intramolecular and intermolecular electronic modulation effects, which play an important role in regulating the reaction energy barrier in the catalytic reaction process. In this section, we will summarize the latest research progress of Ru-based nanomaterials with specific engineering strategies and derived modulated effects in

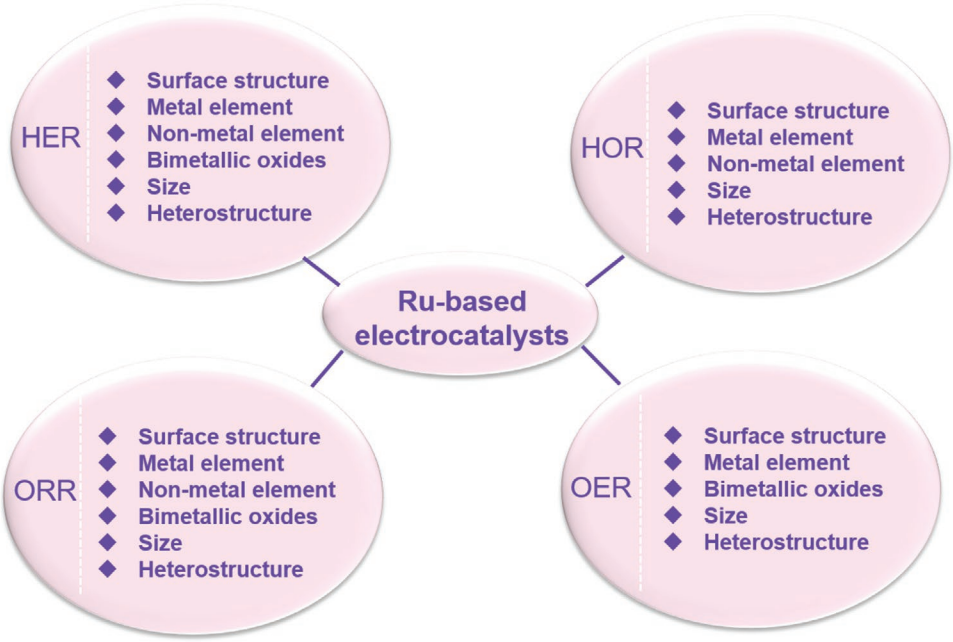

Figure 9. A schematic summary of design strategies of Ru-based electrocatalysts for HER, HOR, ORR, and OER.

hydrogen–oxygen conversion reactions (HER, HOR, ORR, and OER). **Figure 9** shows the schematic summary of design strategies of the Ru-based electrocatalysts for each reaction.

4.1. Hydrogen Evolution Reaction

HER is an important half-reaction in water electrolysis, which requires two electrons to be involved for each H_2 molecule generation.[114] Generally, HER occurs via the Volmer–Heyrovsky or Volmer–Tafel mechanism in acid or alkaline conditions.[115,116] The difference between Heyrovsky and Tafel reactions is that the Heyrovsky reaction is electrochemical desorption, while the Tafel reaction is chemical desorption.[117] According to the Sabatier principle, the free energy of adsorption of H* (ΔG_{H^*}) can be used to evaluate the HER catalytic activity, and the moderate adsorption strength with H* should be achieved for the optimized electrocatalysts. If H* adsorption is too weak, the Volmer reaction will hinder the overall reaction, whereas the adsorption is too strong, the Heyrovsky/Tafel reaction will be the rate-determining step.[118,119] Precious metal Pt catalysts are often used as a benchmark for HER due to their outstanding activity and stability. However, the high price and low distribution block their world-wide application. Ru-based catalysts with much lower price show a similar H-bond strength to Pt, making it promising alternatives to Pt-based HER catalysts.

It is widely accepted that the reaction kinetics of HER can be revealed by Tafel slopes. The Ru-based nanomaterials usually exhibited the Tafel slope in the range of 30–50 mV dec^{-1}, which indicates the HER follows the Volmer–Heyrovsky or Volmer–Tafel mechanisms. The H* binding energy or water adsorption/dissociation energy on Ru-based nanomaterials determines the catalytic ability of HER. All the above-mentioned engineering strategies of Ru-based materials can be applied to achieve excellent HER catalytic activity. For instance, Ru with a specific facet can expose more active sites to lower the reaction energy barrier. Metal/nonmetal element engineering and bimetallic oxide modification strategies can take away electrons from Ru, which promotes the desorption of H* and accelerates the Heyrovsky or Tafel steps in HER process. In addition, the introduction of nonmetallic elements into Ru can also improve the Volmer step to enhance HER activity. The size engineering can maximize the active sites and the heterostructure strategy leads to the charge redistribution, both of which highly affect the adsorption capacity for HER reactants/intermediates and thereby the HER catalytic activity. In this section, we will discuss the various engineering strategies of Ru-based materials for boosted HER.

4.1.1. Surface Structure-Engineered Ru-Based Electrocatalysts for HER

Tuning phase structure of the metallic Ru catalysts can efficiently alter the HER catalytic activity, due to the new derived crystal phase structure and more exposed active sites. The hierarchical 4H/fcc Ru nanotubes (Ru NTs) with ultrathin Ru shells were derived by using novel 4H/fcc Au nanowires with crystalline heterostructure as sacrificial templates (**Figure 10**a). The interface between the two crystal phases (fcc/hcp-4H) results in rich atomic steps and kinks, which effectively tune the local electronic structure of Ru atoms (Figure 10b–d). Moreover, the hierarchical porous structure provides abundant active sites, enabling 4H/fcc Ru NTs with an overpotential of 23 mV at a current density of 10 mA cm^{-2} (Figure 10e,f).[120] The formed superstructure 2D nanosheets with unique lattice mismatch can further engineer the metallic Ru catalysts. The hcp-Ru multilayer nanosheets (Ru MNSs) with superlattice structure have been prepared by wet chemical method with triruthenium dodecacarbonyl ($Ru_3(CO)_{12}$) as the precursor,

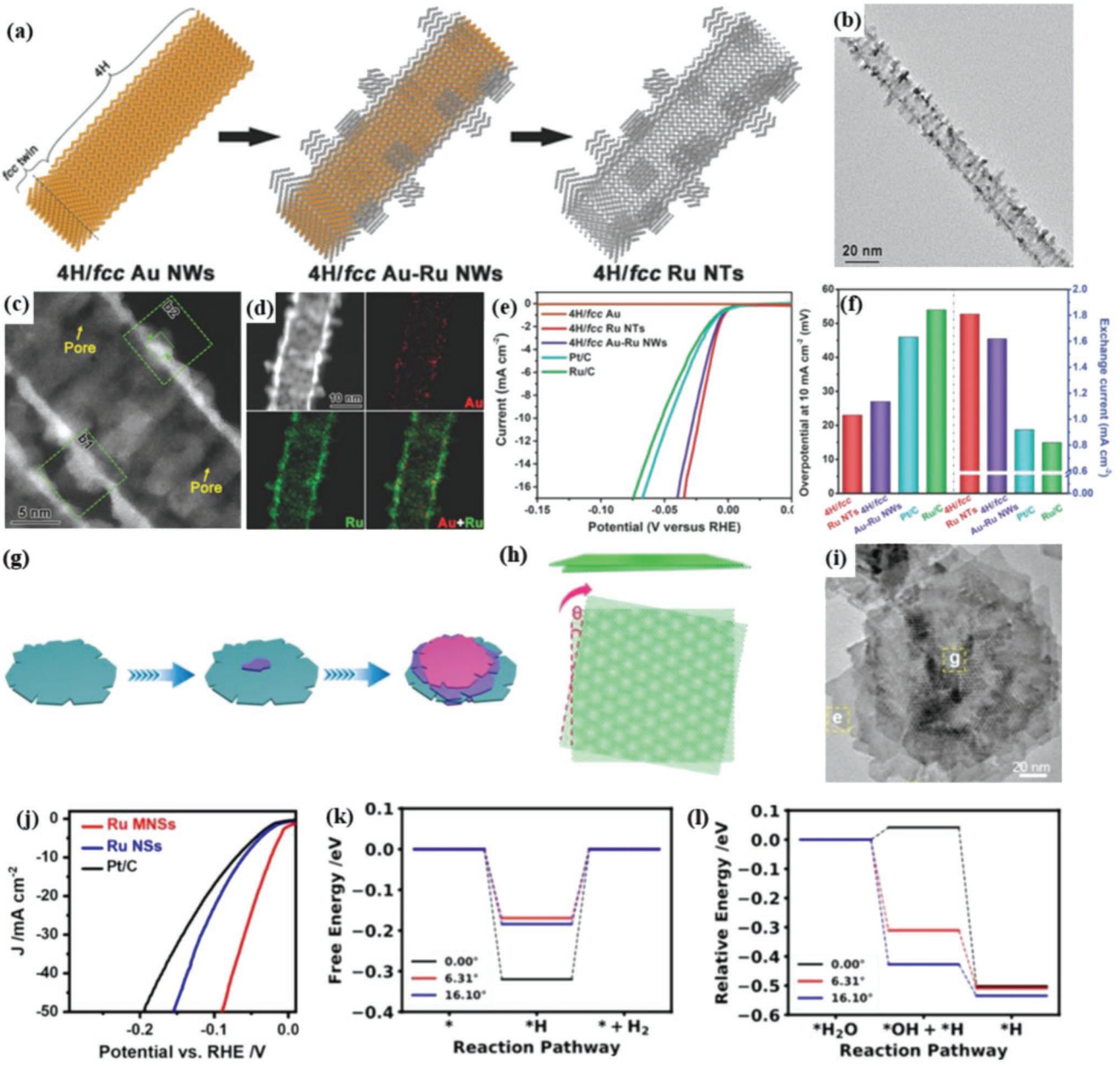

Figure 10. Surface structure and metal element engineering strategies of Ru-based catalysts for HER: a) Scheme of the preparation, b,c) TEM images, and d) STEM elemental mapping of hierarchical 4H/fcc Ru NTs. e) Polarization curves in 1.0 M KOH solution. f) Comparison of overpotentials and exchange current densities between 4H/fcc Ru NTs and comparative materials. Reproduced with permission.[120] Copyright 2018, Wiley-VCH. Surface structure engineering strategies of Ru-based catalysts for HER: g) Formation process and h) 3D and 2D views of the Ru MNSs superlattice model. i) TEM image of Ru MNSs. j) HER polarization curves in 1.0 M KOH. The calculated Gibbs free energies diagram of k) water dissociation and l) HER processes on Ru MNSs. Reproduced with permission.[121] Copyright 2022, Wiley-VCH.

cetyltrimethylammonium bromide (CTAB) and citric acid monohydrate (CA) as structure directing agents, polyvinylpyrrolidone (PVP) as a surfactant. Ultrathin hcp-Ru NSs are stacked by overgrowth with twist angles of 2°–30° to form a Ru-based superlattice structure (Figure 10g–i). As shown in Figure 10j, the superstructure Ru MNSs requires an overpotential of 24 mV to achieve 10 mA cm^{-2} in alkaline HER, which is much lower than those of commercial Pt/C (70 mV) and Ru NSs (61 mV). DFT calculations indicate that the certain twist angle between Ru NSs in the superlattice induces a strain effect, which weakens the adsorption capacity for H* and accelerates the HER process (Figure 10k,l).[121]

4.1.2. Metal Element-Engineered Ru-Based Electrocatalysts for HER

Alloying is another efficient strategy to alter the electronic structure and corresponding catalytic activity of Ru-based catalysts. Alloying Ru with Pd forming Pd_3Ru alloy catalyst with surface Ru segregation (Ru clusters) has been achieved by the

impregnation method. The surface-segregated Ru clusters effectively tune the electronic structure of the catalyst, down-shifting the d-band center and weakening the H* adsorption energy of Ru clusters/Pd_3Ru, thus achieving a smaller HER energy barrier. The experimental results show that the overpotential of Ru clusters/Pd_3Ru is 42 mV at a current density of 10 mA cm^{-2}, lower than that of Pd/C (η = 146 mV).[122] The incorporation of transition metals can modulate the 4d orbital electronic structure of Ru. RuCo alloy nanosheets (RuCo ANSs) were obtained by intercalating Ru into ultrathin Co nanosheets by rapid co-precipitation and in situ electrochemical reduction processes.[123] Compared with pure Ru nanoparticles, the Co atoms in RuCo ANSs make the 4d orbitals of Ru sites plane-symmetric in the *xy*-direction but asymmetric in the *z*-direction, which affects the Ru–H interaction. The orbital of Ru $4d_{Z^2}$ changed significantly after H adsorption, which indicated that Ru $4d_{Z^2}$ was the determining factor for the free energy of hydrogen adsorption. In alkaline solution, RuCo ANSs delivered ultralow overpotential (η = 10 mV) for a current density of 10 mA cm^{-2} and Tafel slope (20.6 mV dec^{-1}). And the achieved turnover frequency of RuCo ANSs is 2 and 15 times higher than those of commercial Pt/C and Ru/C, respectively.

4.1.3. Nonmetal Element-Engineered Ru-Based Electrocatalysts for HER

Nonmetal element can also significantly optimize the electronic properties of Ru-based catalysts. It has been reported that the HER activity of Ru can be awakened with the inert ingredient silicon (Si).[124] The introduction of Si induced the strain and the ligand effects resulting in an optimized electronic structure of Ru atoms. The overpotential η_{10} of RuSi NPs in acidic HER is only 19 mV, and the Tafel slope is 28.9 mV dec^{-1}, which is superior to both of Pt and Ru under the same conditions (**Figure 11**a,b). DFT calculation results demonstrated that the introduction of Si atoms successfully eliminates the Ru_3-hollow sites, which have

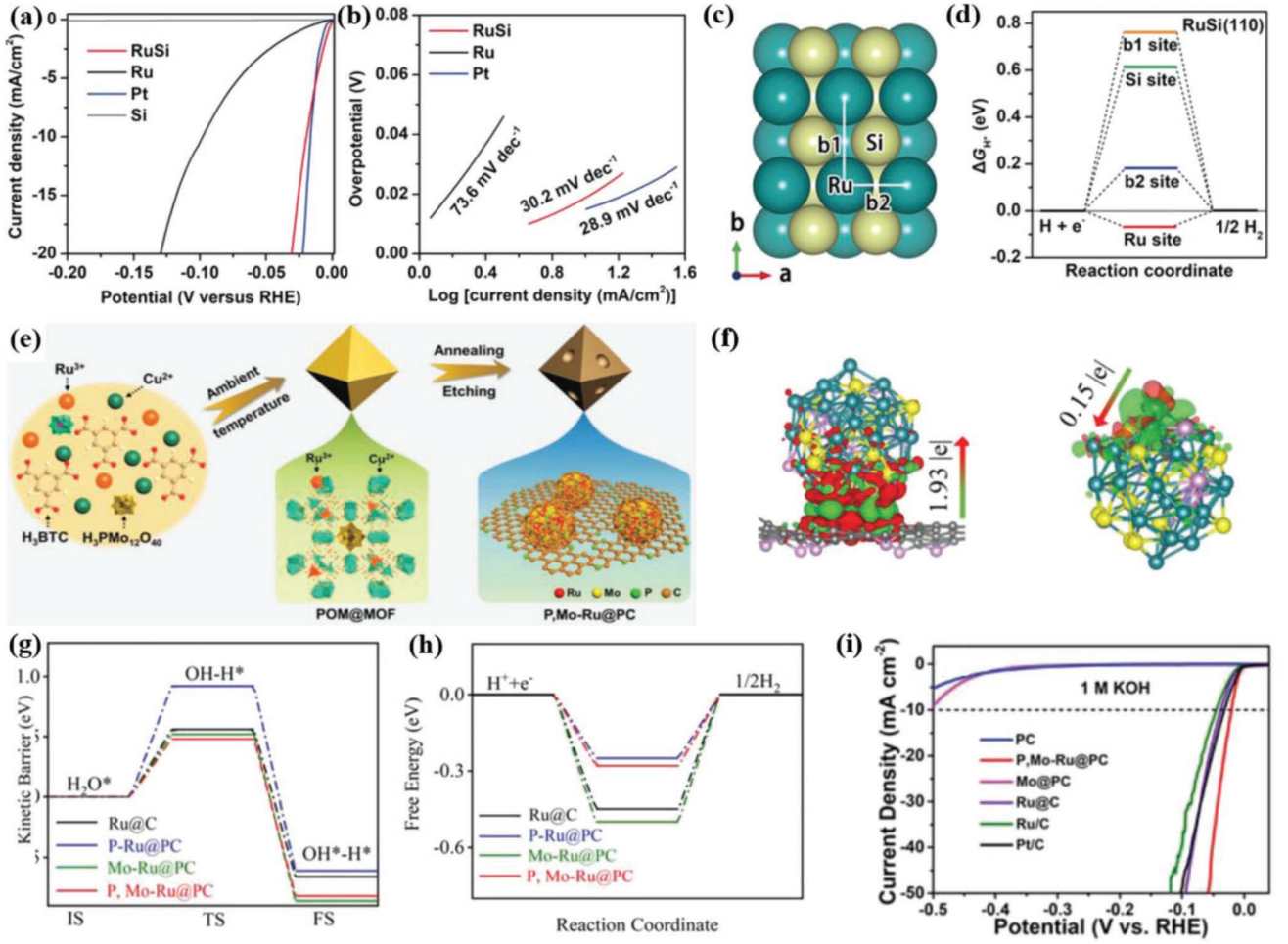

Figure 11. Nonmetal element engineering strategy of Ru-based catalysts for HER: a) Polarization curves and b) Tafel plots of RuSi, Ru, and Pt in 0.5 M H_2SO_4 solution. c) H adsorption sites in RuSi and d) ΔG_{H^*} values on RuSi (110) surface. Reproduced with permission.[124] Copyright 2019, Wiley-VCH. Metal and nonmetal element engineering strategies of Ru-based catalysts for HER: e) Schematic diagram of the preparation process of P,Mo-Ru@PC. f) Distribution of charge density between P,Mo-Ru clusters and PC and individual Ru atoms in P,Mo-Ru clusters. Red represents positive charge and green represents negative charge. g) Gibbs free energy diagrams and h) hydrolysis kinetic energy barriers for HER for different catalysts. IS, TS, and FS correspond to the initial, transition, and final states, respectively. i) Linear sweep voltammetry (LSV) plots of P,Mo-Ru@PC and compared samples. Reproduced with permission.[126] Copyright 2022, Wiley-VCH.

a strong adsorption effect on H*, so that the catalytic activity on the top of Ru sites with moderate H* adsorption strength is revealed (Figure 11c,d). In addition, incorporating nonmetal element forming Ru-compounds, such as RuP, RuB_2, may induce the d-sp orbital hybridization, which can lead to the down-shift of the d-band center and optimize the adsorption of H*. In acidic and alkaline media, RuB_2 ($\eta_{10,\ acid}$ = 18 mV, $\eta_{10,\ alkaline}$ = 28 mV) showed comparable or even superior catalytic activity to commercial Pt/C ($\eta_{10,\ acid}$ = 17 mV, $\eta_{10,\ alkaline}$ = 37 mV).[125]

Dual doping of nonmetallic and metallic heteroatoms can synergistically improve the intrinsic activity of Ru-based catalysts. P, Mo dual-doped Ru ultrasmall nanoclusters dispersed on P-doped porous carbon (P, Mo-Ru@PC) have been achieved by in situ self-assembly, and co-precipitation, annealing, and etching treatments (Figure 11e). Excess electrons were transferred from Ru to Mo and P heteroatoms, leading to the positive charge of Ru atoms, which accelerates the water dissociation and reduces H* adsorption energy (Figure 11f–h). P, Mo-Ru@PC exhibits low alkaline HER overpotential (η_{10} = 21 mV) in Figure 11i compared to the Ru@C without Mo and P (η_{10} = 38 mV).[126]

4.1.4. Bimetallic Oxides-Engineered Ru-Based Electrocatalysts for HER

The introduction of metal elements into RuO_2 can not only increase the active sites of HER, but also increase the oxygen defects to adjust the d-band center of Ru-based bimetallic oxides and optimize the H* binding ability. For instance, the introduction of the corrosion-resistant metal Pt into RuO_2 can provide new active sites for HER as Pt is regarded as a benchmark catalyst in acidic conditions. A trace amount of Pt (5%) was introduced into Ru nanosheet assemblies (Ru NAs) by "one-pot" approach and 5%Pt-Ru oxide nanosheet assemblies (Pt-Ru ONAs/C) have been achieved after annealing. The oxidized Ru and Pt species on the surface of 5%Pt-Ru ONAs/C have been reduced to their metallic states in the acidic HER process, which efficiently increased the active sites and promoted the hydrogen generation. The overpotentials (η_{10}) of 5%Pt-Ru ONAs/C in 0.5 and 0.05 M H_2SO_4 are 31 and 40 mV, respectively, which are better than those of undoped Ru ONAs/C (η_{10} = 53 and 59 mV).[127] In addition, the rare earth metal ions La^{3+} can also effectively increase the oxygen vacancies and tune the electronic structure of RuO_2, thereby reducing the d-band center of La-RuO_2 and further weakening the adsorption of H*. In an acidic medium, La-RuO_2 delivered a low overpotential of 71 mV at a current density of 10 mA cm^{-2}, which is much lower than that of commercial Pt/C (85.7 mV), La-RuO_2 also exhibited excellent stability with no degradation during the 50 h chronopotentiometry test.[128]

4.1.5. Size-Engineered Ru-Based Electrocatalysts for HER

The catalytic activity is closely related to the exposed active sites on the catalyst surface, and the number of active sites can be increased by reducing the size of Ru NPs to facilitate the catalytic reaction. Therefore, the HER catalytic activity shows a high dependence on the size of Ru NPs. For example, a series of Ru/C particles with various particle sizes were prepared by the low-temperature pyrolysis method. Among them, Ru/C-300 has the smallest average size of 1.48 nm, showing the highest alkaline HER catalytic activity (η_{10} = 14 mV), whereas Ru/C-400 (particle size of 1.55 nm, η_{10} = 15 mV), Ru/C-500 (particle size of 1.63 nm, η_{10} = 25 mV), and Ru/C-700 (particle size of 4.72 nm, η_{10} = 31 mV) deliver relatively lower catalytic activities.[129] Shrinking nanoparticles down to the atomic scale is the most efficient way to increase atomic utilization. Furthermore, the single metal atoms with new electronic states and uncoordinated properties endow the excellent catalytic performance. For example, Ni_5P_4-Ru electrocatalysts with monodispersed Ru atoms were prepared by using a nickel vacancy-mediated synthesis impregnation-phosphating method (**Figure 12**a).[130] The interaction of monatomic Ru with Ni_5P_4 increases the local electron density of Ru atoms, which accelerates the HER process and weakens the H* adsorption energy (Figure 12b,e,f). In 1.0 M KOH solution, the overpotential for the current density of 10 mA cm^{-2} of Ni_5P_4-Ru is 123 mV lower than that of the support Ni_5P_4, and the catalytic activity is still maintained after 10k cycles (Figure 12c,d). In addition, the co-existence of Ru SAs and NPs can also accelerate the HER process through the synergistic effect. For example, Song et al.[131] prepared $Ru_{1,n}$-NC with the presence of Ru NPs and SAs by the pyrolysis of Ru-supported polypyrrole at high temperature (Figure 12g,h). In 1.0 M KOH solution, the overpotential (η_{10}) of $Ru_{1,n}$-NC is only 14.8 mV, which is lower than those that of Ru/NC (61.1 mV) and Ru_1-NC (152.3 mV) loaded with only Ru NPs and Ru SAs, respectively (Figure 12i). The interaction of Ru_{NP} and Ru_{SA} in $Ru_{1,n}$-NC reduced OH* desorption capacity on Ru_{NP} and H* desorption capacity on Ru_{SA}, respectively, resulting in stronger water adsorption and proton accumulation capacity of $Ru_{1,n}$-NCs, which accelerate the HER process (Figure 12j–m).

4.1.6. Heterostructure-Engineered Ru-Based Electrocatalysts for HER

The construction of heterostructure with well-defined interfaces is considered as an efficient approach to increase intrinsic catalytic activity. The redistribution of charges across the interface provides an opportunity to optimize the electronic structure of the catalyst, thereby affecting the adsorption capacity for active intermediates. For example, heterostructured Ru-Ru_2P and the comparison counterparts (pure Ru and Ru_2P species) were fabricated by electrospinning technique with polyacrylonitrile (PAN) nanofibers containing polyphytic acid (PA) and Ru^{3+} as precursors. The achieved Ru-Ru_2P@CNFs exhibited outstanding acidic (η_{10} = 11 mV) and alkaline (η_{10} = 14 mV) HER catalytic behaviors, which is much superior compared to the pristine Ru (η_{10} = 153 mV) and Ru_2P (η_{10} = 25 mV). The high HER catalytic activity is ascribed to the charge redistribution at the heterointerface of Ru and Ru_2P, which optimizes the electronic structure and promotes the electrical conductivity, enabling a near-zero H* adsorption strength (ΔG_{H^*} = 0.034 eV) of Ru-Ru_2P@CNFs.[132] Moreover, the introduction of an amorphous phase in the construction of heterostructure may result in an unsaturated coordination environment, increasing the adsorption capacity for reactive intermediates. The amorphous RuCu nanosheets (RuCu NCs) in situ grown on crystalline Cu nanotubes formed

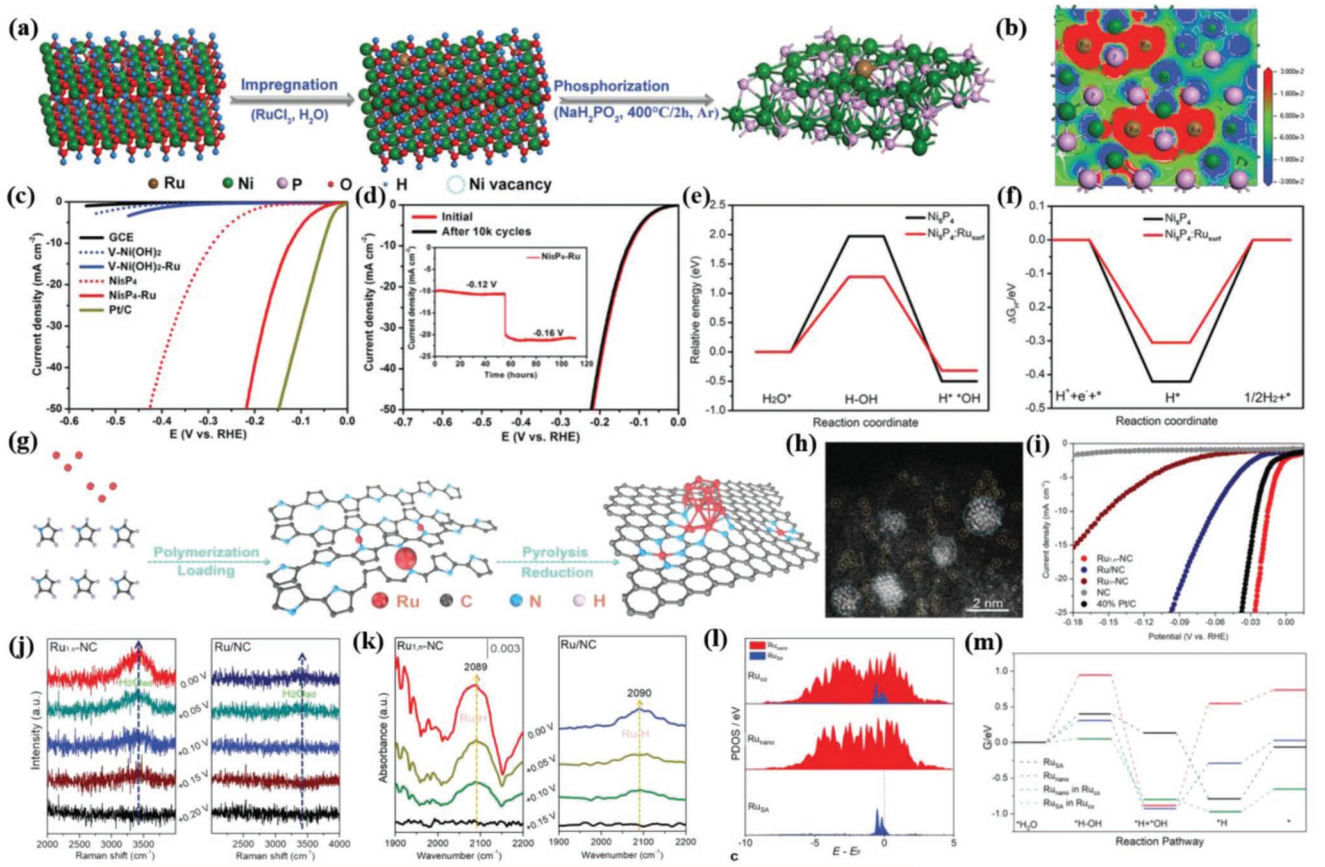

Figure 12. Size engineering strategies of Ru-based catalysts for HER: a) Schematic diagram of the synthesis of Ni_5P_4-Ru. b) Bader analysis. c) LSV curve measured in 1.0 M KOH solution. d) LSV curves after CV cycling at a given potential (inset is chronoamperometry). e) Water dissociation energies and f) H* adsorption energies of Ni_5P_4-Ru and Ni_5P_4. Reproduced with permission.[130] Copyright 2020, Wiley-VCH. g) Flow chart of the preparation of $Ru_{1,n}$-NC and h) HAADF-STEM image. i) LSV polarization curves of $Ru_{1,n}$-NC and comparative samples. j) In situ Raman and k) in situ SR-IRAS analysis. l) PDOS analysis and m) free energy during HER process picture of bare Ru_{SA}, Ru_{NP}, and Ru_{co} ($Ru_{1,n}$-NC). Reproduced with permission.[131] Copyright 2022, Wiley-VCH.

a special amorphous-crystalline heterostructure, which enables 3D RuCu NCs with HER overpotentials of η_{10} = 18 and 73 mV in alkaline and neutral media, respectively (**Figure 13**a–d). The unsaturated bonds on amorphous RuCu facilitated the adsorption of reactants, and the crystalline Cu nanotubes efficiently increased the electrical conductivity (Figure 13e), which synergistically promoted the HER process.[133] **Table 1** summarizes the HER activity of various Ru-based electrocatalysts.

4.2. Hydrogen Oxidation Reaction

HOR is an important anode reaction involved in AEMFCs. HOR is the reverse process compared to HER, and the reaction steps also include Tafel, Heyrovsky, and Volmer processes. The Tafel/Heyrovsky reaction is to dissociate H_2 into H*, and then the Volmer reaction facilitates the formation of H_2O molecules.[116] It is believed that the adsorption strength of H* and OH* intermediates on the catalyst jointly determines the reaction rate of HOR in alkaline media.[134]

HOR usually processes through Tafel–Volmer or Heyrovsky–Volmer pathways. Ru has strong binding strength to both H* and OH*, which is unfavorable for the desorption of H*, and the accumulated large amounts of OH* occupy the active sites.[15] Ultimately, Ru needs to overcome a large reaction energy barrier to complete the recombination of H* and OH* to form water (Volmer reaction), which is usually the rate-determining steps. Therefore, metal or nonmetal element modification is usually selected to prepare Ru-based nanomaterials as HOR electrocatalysts. The introduction of metal elements to alloy with Ru usually results in electronic modulation effects, so that the doped metal elements and Ru are active for H* and OH*, and accelerate the generation of H_2O. Second, the introduction of nonmetal heteroatoms shifts the d-band center of Ru-based nanomaterials down, which not only weakens the OH* adsorption but also optimizes the H* binding capacity, thereby accelerating the Volmer reaction of HOR.

4.2.1. Surface Structure-Engineered Ru-Based Electrocatalysts for HOR

Elaborate design of the morphology and structure of Ru-based catalysts can increase the HOR catalytic activity and stability. Chain-like porous Ru nanoparticles on carbon supports (Ru/C) allow more

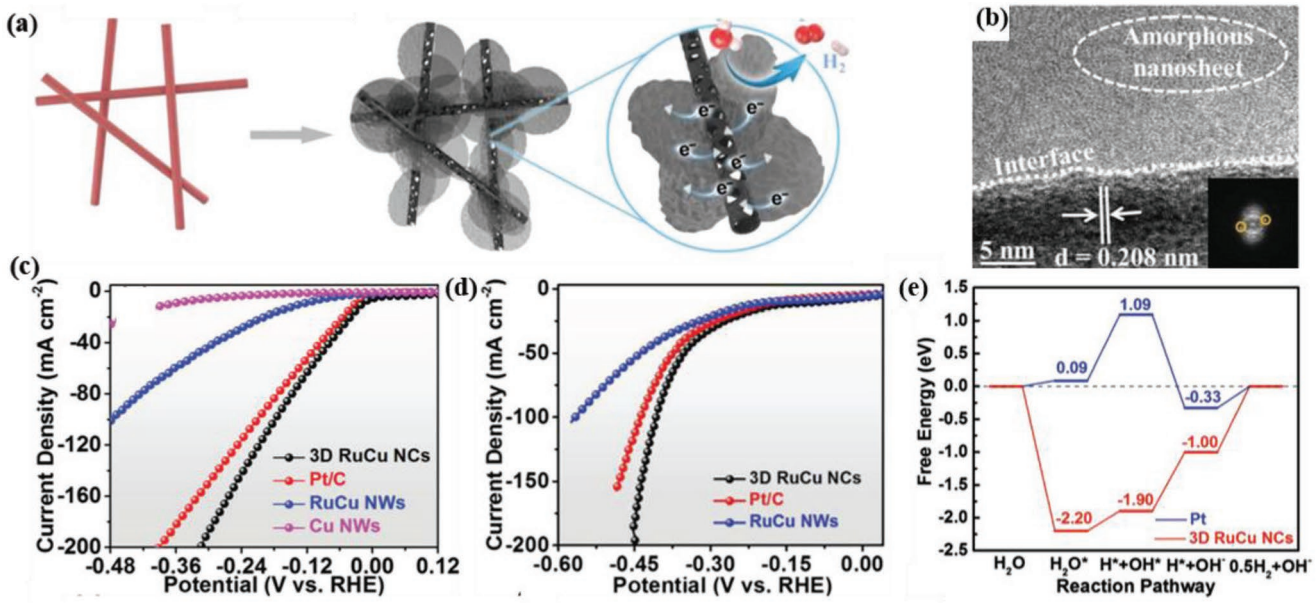

Figure 13. Heterostructure engineering strategies of Ru-based catalysts for HER: a) Synthetic route and b) TEM image of 3D RuCu NCs. HER polarization curves in c) 1.0 M KOH and d) 0.01 M PBS solutions. e) Free energy diagram of HER. Reproduced with permission.[133] Copyright 2020, Wiley-VCH.

Ru sites to be exposed to facilitate the HOR process at various pH conditions.[135] Furthermore, Ru nanoparticles confined in the TiO_2 lattice (Ru@TiO_2) resulted in a unique confinement effect, weakening the adsorption of OH* and H* simultaneously, allowing more active sites to be released and increasing both the kinetics and stability of HOR. Ru@TiO_2 delivered high HOR mass activity in acidic and alkaline media ($MA_{acid} = 380\,A\,g_{Ru}^{-1}$ and $MA_{alkaline} = 282\,A\,g_{Ru}^{-1}$), which are 15–30% superior to that of PtRu catalyst ($MA_{acid} = 300\,A\,g_{precious\ metal}^{-1}$ and $MA_{alkaline} = 244\,A\,g_{precious\ metal}^{-1}$).[136]

4.2.2. Metal Element-Engineered Ru-Based Electrocatalysts for HOR

To further enhance the HOR catalytic activity, Ru can be alloyed with metal elements for optimized charge transfer. For example, the ultrathin IrRu alloy nanowire networks (IrRu NWs/C) lead to the electron transfer between Ru and Ir, reducing the adsorption strength of H*, and the oxidized Ru on the surface reduces the adsorption strength of OH*, which simultaneously boost the reaction rate of HOR. When successfully applied in alkaline

Table 1. The engineered Ru-based electrocatalysts for HER.

Catalysts	Modification strategy	Loading [mg cm^{-2}]	Electrolytes	η_{10} [mV vs RHE]	Tafel slope [mV dec^{-1}]	Ref.
4H/fcc Ru NTs	Surface structure	0.034	1.0 M KOH	23	34	[120]
Ru MNSs	Surface structure	0.1	1.0 M KOH	24	33.8	[121]
Pd_3Ru	Metal element	0.015	1.0 M KOH	42	–	[122]
RuCo ANSs	Metal element	–	1.0 M KOH	10	20.6	[123]
RuSi NPs	Nonmetal element	0.562	0.5 M H_2SO_4	19	30.2	[124]
RuB_2	Nonmetal element	0.281	1.0 M KOH	28	28.7	[125]
			0.5 M H_2SO_4	18	38.9	
P,Mo-Ru@PC	Metal +Nonmetal	–	1.0 M KOH	21	21.7	[126]
5%Pt-Ru ONAs/C	Bimetallic oxides	14.14 wt%	0.5 M H_2SO_4	31	32.4	[127]
			0.05 M H_2SO_4	40	39.7	
La-RuO_2	Bimetallic oxides	–	0.5 M H_2SO_4	71	49.3	[128]
Ru/C-300	Size	–	1.0 M KOH	14	32.5	[129]
Ni_5P_4-Ru	Size	0.142	1.0 M KOH	123	56.7	[130]
$Ru_{1,n}$-NC	Size	–	1.0 M KOH	14.8	22.3	[131]
Ru-Ru_2P@CNFs	Heterostructure	0.26	1.0 M KOH	11	24.2	[132]
			0.5 M H_2SO_4	14	24.5	
RuCu NCs	Heterostructure	–	1.0 M KOH	18	59	[133]
			0.01 M PBS	73	314	

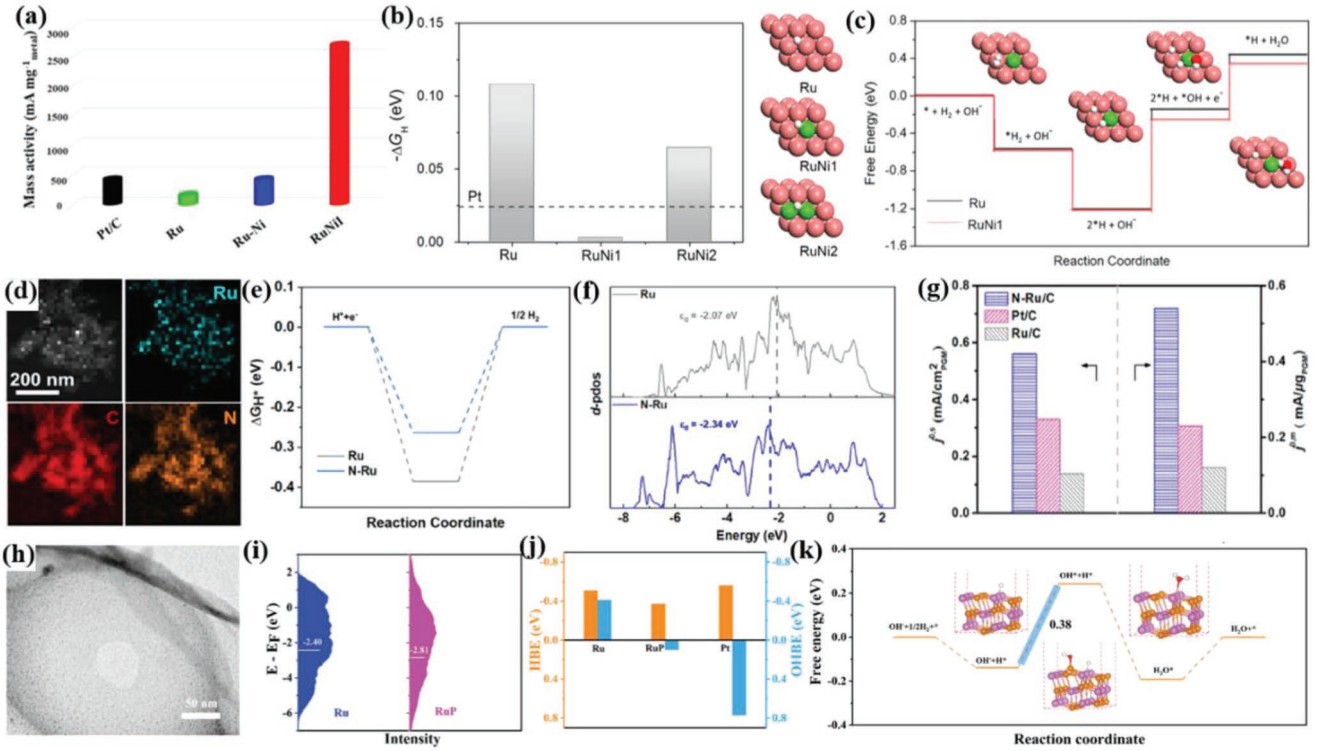

Figure 14. Surface structure and metal element engineering strategies of Ru-based catalysts for HOR: a) MA at 50 mV (vs RHE) overpotential. b) Hydrogen adsorption energies on pure ruthenium, monoatomic nickel, and diatomic nickel dispersed over a ruthenium catalyst, with orange: ruthenium; green: nickel; red: oxygen; white: hydrogen. c) Free energy diagram of the HOR process. Reproduced with permission.[138] Copyright 2020, American Chemical Society. Nonmetal element engineering strategies of Ru-based catalysts for HOR: d) EDX elemental mapping of Ru and N in N-Ru/C. e) The free energy of hydrogen adsorption (ΔG_{H^*}) on N-Ru and pure Ru and f) the corresponding d-PDOS of Ru. g) MA and specific activity (SA) in 0.1 M KOH. Reproduced with permission.[139] Copyright 2021, Elsevier. h) TEM image of RuP/NOC. i) The d-band center of Ru in Ru and RuP. j) HBE and OHBE of Ru, RuP, and Pt. k) Free energy diagrams of intermediates in the HOR process on RuP (011). Reproduced with permission.[140] Copyright 2022, Wiley-VCH.

AEMFC, IrRu NWs/C achieved a peak power density of over 485 mW cm^{-2} activity.[137] In addition, monodispersed transition metal atoms can also be introduced to the Ru lattice, and the electronic structure of Ru can be precisely tuned at the atomic level. The combination of Ru nanosheets with surface-dispersed Ni single-atom ($RuNi_1$ NCs) can effectively promote HOR.[138] Monodispersed Ni atoms reduced the H* binding energy and water formation energy barriers on Ru nanocrystals (**Figure 14**b,c). In alkaline electrolytes, the HOR mass activity of $RuNi_1$ NCs is 6.3 times higher than those of Ru-Ni NCs and commercial Pt/C, and 16.6 times of Ru catalysts, respectively (Figure 14a).

4.2.3. Nonmetal Element-Engineered Ru-Based Electrocatalysts for HOR

The introduction of nonmetal heteroatoms (e.g., N, P, S, etc.) into the Ru lattice leads to enhanced HOR catalytic activities due to the electron transfer from Ru to nonmetal heteroatoms, resulting in optimized adsorption of H* and OH*. For example, doping N atoms into Ru nanoparticles (N-Ru/C) can be realized under NH_3 atmosphere, and the electron transfer from Ru to N makes Ru have a moderate adsorption strength of H* and the down-shifted d-band center (Figure 14e,f). As the results shown in Figure 14g, the mass activity and exchange current density of N-Ru/C in 0.1 M KOH are 4.5 and four times higher than that of Ru/C, respectively.[139] The effect of phosphating on the HOR catalytic activity of Ru-based materials is similar to the above N effect. The RuP nanoparticles were successfully constructed on N and O co-doped 3D porous hollow carbon substrates (RuP/NOC) (Figure 14h). The kinetic mass activity of RuP/NOC is 13 times higher than that of commercial Pt/C at the overpotential of 50 mV. Similar to the N effect, the electron transfer from Ru to P causes the down-shift of the Ru d-band center (Figure 14i), which is contributed to the excellent HOR catalytic activity in alkaline solution. Moreover, the phosphating could weaken the adsorption of OH* on the catalyst surface, decreasing the reaction energy barrier of $\Delta G = 0.38$ eV, which is smaller than that of RDS (H_2O formation reaction, $\Delta G = 0.44$ eV) in the Ru-catalyzed HOR process (Figure 14j,k).[140] Furthermore, amine ligands can provide N atoms to tune the local electron density of Ru at the molecular level. Ultrasmall-sized (average size of 1.45 nm) Ru nanoclusters are dispersed on an amine ligand-modified carbon support (Ru/PEI-XC). The metal mass-normalized kinetic activity (j_k) of Ru/PEI-XC (j_k = 423.3 A g_{metal}^{-2}) in H_2-saturated 0.1 M KOH is 1.2 and 1.7 times higher than those of Ru/XC (j_k = 373.9 A g_{metal}^{-2}) and Pt/C (j_k = 249.0 A g_{metal}^{-2}), respectively. The interaction of Ru with NH_2 moves the d-band center down, which not only promotes H* adsorption but also weakens the adsorption of OH*, facilitating HOR process.[141]

4.2.4. Size-Engineered Ru-Based Electrocatalysts for HOR

Small-sized nanoparticles usually expose unsaturated metal atoms on the surface, which is beneficial for catalytic reactions. It is found that the alkaline HOR activity showed a volcanic relationship with the size of Ru NPs. The results demonstrated that Ru changed from an amorphous structure (below 3 nm) to a crystalline structure (above 3 nm), and Ru metal nanocrystalline particles with an amorphous capping layer with an average particle size of 3 nm show a high proportion of unsaturated atoms, exhibiting the highest mass activity.[142] Further reducing the size of the Ru catalyst to the atomic level can greatly improve the atomic utilization and catalytic capability. Ru single atoms anchored on N, S-doped porous graphene (RuSA/NSG) is an efficient HOR electrocatalyst. The Ru atoms are coordinated with N and S forming Ru-N_4-S_2 atomic structure as the active center, showing low H* adsorption energy and water formation energy, which makes the mass activity 6.1 and 3.5 times higher than those of Ru/C and Pt/C, respectively.[143]

4.2.5. Heterostructure-Engineered Ru-Based Electrocatalysts for HOR

On the basis of the PtRu bifunctional mechanism, the use of a heterostructure composed of RuO_2 and Pt with stronger oxidophilicity can further promote HOR process. The heterojunction Pt-RuO_2 catalyst exhibited superior current density in 0.1 M NaOH and 0.1 M benzyl trimethylammonium hydroxide (BTMAOH) electrolytes. The presence of RuO_2 and the unique heterojunction interface of Pt-RuO_2 boosted the catalytic activity of HOR and the mass transfer of H_2, exhibiting excellent AEMFC performance with peak power densities of 0.77 W cm^{-2} and specific powers of 31 W mg_{Pt}^{-1}.[144]

4.3. Oxygen Reduction Reaction

The ORR is a proton-electron transfer process that reduces oxygen to water through direct four-electron reactions or hydrogen peroxide (H_2O_2) by two-electron reactions.[145] ORR involves in cathode reactions in fuel cells, and direct four-electron transfer is an ideal reaction pathway. The two-electron pathway provides a green synthesis route for H_2O_2, ascribing to the considerable application value for wastewater treatment and disinfection.[146] Oxygen-containing intermediates (OOH*, O*, OH*, etc.) are generated during the ORR process, and theoretical calculations demonstrate that the adsorption strength of these intermediates on active sites should be neither too strong nor too weak to be favorable for ORR.[147] Recently, Ru-based materials have been investigated as efficient catalysts for ORR.

The strong affinity between Ru and O species can promote the ORR process. The surface properties of metallic Ru, RuO_2, or hydrated RuO have a certain effect on the adsorption of O species, which can influence the reaction kinetics. For instance, metallic Ru prefers to reduce O_2 to H_2O/OH^- via a direct $4e^-$ process, whereas a $2e^-$ reduction process occurs on the hydrated oxides to generate H_2O_2.[148] The reduction step of OH* was usually the rate-determining step for Ru-based nanomaterials, which is consistent with the rate-controlling step of metal Pt-catalyzed ORR.[149] The Ru single-atom catalysts are one kind of widely investigated ORR electrocatalysts. The atomically dispersed Ru coordinated with the heteroatoms are the active centers for ORR. These heteroatoms effectively tune the d-band center of the Ru atoms, weakening the Ru—O bond interaction, and thus achieving the optimized adsorption energy of oxygen-containing intermediates.[150] Ru-based nanomaterials obtained by alloying Ru with other metals or constructing heterostructures are also important for ORR, in which the local electronic structure of Ru could be effectively tuned by charge redistribution, reducing the reaction energy barrier of ORR.

4.3.1. Surface Structure and Metal Element-Engineered Ru-Based Electrocatalysts for ORR

Surface structure and metal element engineering strategies of Ru-based materials have been widely studied for ORR. Morphology design coupling with alloying not only increases accessible active sites and accelerates mass transport, but also optimizes the electronic structure of the catalyst to improve the adsorption of active intermediates. For instance, PdAuRu ternary alloy nanospine (PdAuRu NSAs) materials with unique 3D hyperbranched structures exposed more active sites and formed strong electronic interaction between Pd-Au-Ru atoms. The achieved optimized binding energy of O* led to superior mass activity and specific activity of PdAuRu NSAs compared to those of PdAuRu NPs, Pt/C, and Pd/C.[151] Inexpensive transition metal Fe, Co, Ni, etc., alloyed with Ru can improve the charge distribution and surface properties of Ru to promote the intrinsic activity of Ru-based catalysts. The as-prepared RuFe alloy nanoparticles embedded nitrogen-doped porous carbon (RuFe@NC-900) has exhibited excellent alkaline ORR catalytic activity by achieving $E_{1/2}$ at 0.85 V vs RHE and excellent performance in Li-O_2 (the discharge specific capacity is 11129 mAh g^{-1}) and Zn–air batteries (the discharge specific capacity is 751 mAh g_{Zn}^{-1}).[152] Furthermore, Ru as dopants in Ru-doped Ru-Pt_3Co octahedral alloy nanoparticles (Ru-Pt_3Co/C) can effectively inhibit the dissolution of Co and suppress the excessive reduction of Pt during ORR process, which highly boost the catalytic activity and stability. DFT calculations showed that the introduction of Ru further improves the charge distribution of Ru-Pt_3Co/C, which not only accelerates the dissociation of O_2 but also promotes the desorption of the *OOH intermediate, achieving superior mass activity of 7.5 times compared to that of commercial Pt/C.[9]

4.3.2. Nonmetal Element-Engineered Ru-Based Electrocatalysts for ORR

Nonmetal atoms (N) hybridized with Ru forming a novel hypercoordinate RuN_2 monolayer have been investigated as ORR electrocatalyst by theoretical calculations. The results demonstrated the accumulation of a large number of positive charges on the surface of RuN_2 monolayer could fully activate the O_2 molecule to be reduced to H_2O through the 4e process, achieving a half-wave potential of 0.93 V vs RHE, which is about 0.1 V higher than that of commercial Pt/C.[153]

4.3.3. Bimetallic Oxides-Engineered Ru-Based Electrocatalysts for ORR

In Ru-based bimetallic oxides, the electronic interaction of Ru, doped metal, and O atoms highly enhances the intrinsic ORR catalytic activity.[154] For instance, the metallic Mn can be used as a key element to efficiently improve the ORR catalytic activity of RuO_2. These Mn atoms are uniformly dispersed in the lattice of RuO_2 and enriched in the outer part to form a Mn-rich shell, which alters the Mn and Ru atoms on the surface to show lower oxidation states compared to those in the inner part, thereby inducing unpaired d electrons, higher surface reactivity, and optimized OH* binding energy. Therefore, Ru-based bimetallic oxides (Mn-RuO_2) exhibited the half-wave potential ($E_{1/2}$) of 0.86 V vs RHE in 0.1 M KOH, which is much superior to those of pure MnO_2 (0.79 V vs RHE), RuO_2 (0.6 V vs RHE), and commercial Pt/C catalyst (0.85 V vs RHE).[155]

4.3.4. Size-Engineered Ru-Based Electrocatalysts for ORR

Downsizing the size of the catalyst to the single-atom scale exposes more active sites and alters the local electronic structure of SACs under the interaction of metal atoms and substrates, maximizing the utilization efficiency of each atom. The substrates for anchoring Ru single atoms can be classified into carbon materials and noncarbon materials. Both of them can stabilize the Ru single atoms by forming the Ru-light atom or Ru-metal atom bonds. The large specific surface area and electrical conductivity of heteroatom-doped carbon substrates can enable high loading and accelerate the electron transfer of Ru-based SACs. High-temperature treatment of Zn-based gel-sealed activated carbon spheres (ACSs) containing Ru^{3+} resulted in Ru-SA@N-ACS catalysts with the edged N atoms coordinated with Ru atoms (Ru-N_4) (**Figure 15**a–c). The Ru-N_4 center as the active sites enable electron transfer from N to Ru atoms, boosting their intrinsic activity. In addition, Ru-N_4 located at the edge sites showed lower binding energy of oxygen-containing intermediates than the ones at the basal plane, which further increased the ORR activity (Figure 15e). The ORR polarization curves in Figure 15d show that Ru-SA@N-ACSs has the most positive half-wave potential ($E_{1/2}$ = 0.86 V vs RHE).[156] The noncarbon substrates, such as MXenes, with high electrical conductivity and hydrophilicity properties are suitable to support Ru single atoms for ORR. The Ru single atoms stabilized on $Ti_3C_2T_x$ MXene nanosheets (Ru-SA/$Ti_3C_2T_x$) has been achieved and the atomically dispersed Ru were stabilized by oxygen-containing surface functional groups forming Ru-O_2 atomic structure, which highly reduced the reaction energy barrier of RDS (H_2O formation) (Figure 15f,g). The ORR half-wave potential of Ru-SA/$Ti_3C_2T_x$ in acidic solution is 0.80 V versus RHE and the mass activity is 1.77 A mg^{-1} (Figure 15h).[157]

4.3.5. Heterostructure-Engineered Ru-Based Electrocatalysts for ORR

Subverting the conventional metal-support loading strategy to achieve RuO_x-on-Pd nanosheets heterostructure by depositing metal oxide (RuO_x) on metal (Pd) support in reverse thinking.[158] This unique structural design amplifies the interaction of RuO_x and Pd, allowing a large number of charges to accumulate on the atomically dispersed dense RuO_x and Pd NSs substrates, which not only promotes the activation of $*O_2$ and the cleavage of the O—O bond, but also optimizes the binding energy of O* and accelerates the kinetics of the ORR process. In alkaline electrolyte, the half-wave potential $E_{1/2}$ of RuO_x-on-Pd NSs is 0.93 V vs RHE, and the mass activity is eight and 22.4 times higher than those of Pt/C and Pd/C, respectively. The peak power densities of RuO_x-on-Pd in methanol fuel cells (DMFCs) and zinc–air batteries are 233 and 172 mW cm^{-2}, respectively, which both show great potential for application. In addition, the Mott–Schottky heterojunction catalyst composed of Ru and semiconductor materials can also significantly boost the ORR activity. The surface sulfur-vacancy (Vs)-modified Ru/$ZnIn_2S_4$ (Ru-ZIS-Vs) Mott–Schottky heterojunction catalysts have been fabricated by hydrothermal reaction and subsequent $NaBH_4$ reduction.[159] The existence of surface sulfur-vacancies enables a better connection between $ZnIn_2S_4$ (ZIS) and Ru, strengthening the interfacial effect of the Mott–Schottky heterojunction. The heterostructure in Ru-ZIS-Vs forms an electron transport bridge, which not only effectively tunes the electronic structure and energy band positions, but also accelerates the electron transfer. Under the synergistic effect of Ru and semiconducting ZIS, Ru-ZIS-Vs exhibited a small ORR onset potential, a large discharge capacity of 3532 mAh g^{-1}, and increased cycling life (321 cycles) in Li-O_2 batteries. **Table 2** summarizes the ORR activity of various Ru-based electrocatalysts.

4.4. Oxygen Evolution Reaction

OER, an important half-reaction for water splitting and rechargeable metal–air batteries, plays a crucial role in advancing the development of energy conversion devices. Since OER is an endothermic reaction involving four electrons, it is necessary to select suitable electrocatalysts to accelerate the kinetics.[160] Similar to ORR, the OH*, O*, and OOH* intermediates are also involved in the OER reaction process, and usually the formation of the intermediates of O* or OOH* is the rate-control step. Therefore, the bonding ability of catalysts to oxygen-containing intermediates is crucial for OER.[160,161] Currently, RuO_2 is considered as the benchmark catalyst for OER. However, there are still shortcomings for RuO_2 directly used for OER such as poor stability and easy oxidative dissolution at high operating potentials.[33] Therefore, the rational design of Ru-based nanomaterials is desired to optimize the adsorption energy of intermediates to increase the OER activity and stability.

In the volcano relationship diagram of $-\eta_{OER}$ and $\Delta G_{O*}-\Delta G_{OH*}$, RuO_2 shows high OER catalytic ability near the volcano peak. It has been demonstrated that the O bridged on the (110) crystal face of RuO_2 could function as a proton acceptor, which facilitated the adsorption/desorption of OER intermediates.[162] RuO_2 undergoes different OER reaction pathways depending on the applied voltage. At low voltage, RuO_2 follows the traditional adsorbate evolution mechanism (AEM), and the O atoms in the generated O_2 are all derived from water. In contrast, lattice O (O_{lat}) in RuO_2 couples with adsorbed O (O_{ad}) to release O_2 at high voltage, which follows the lattice oxygen mechanism

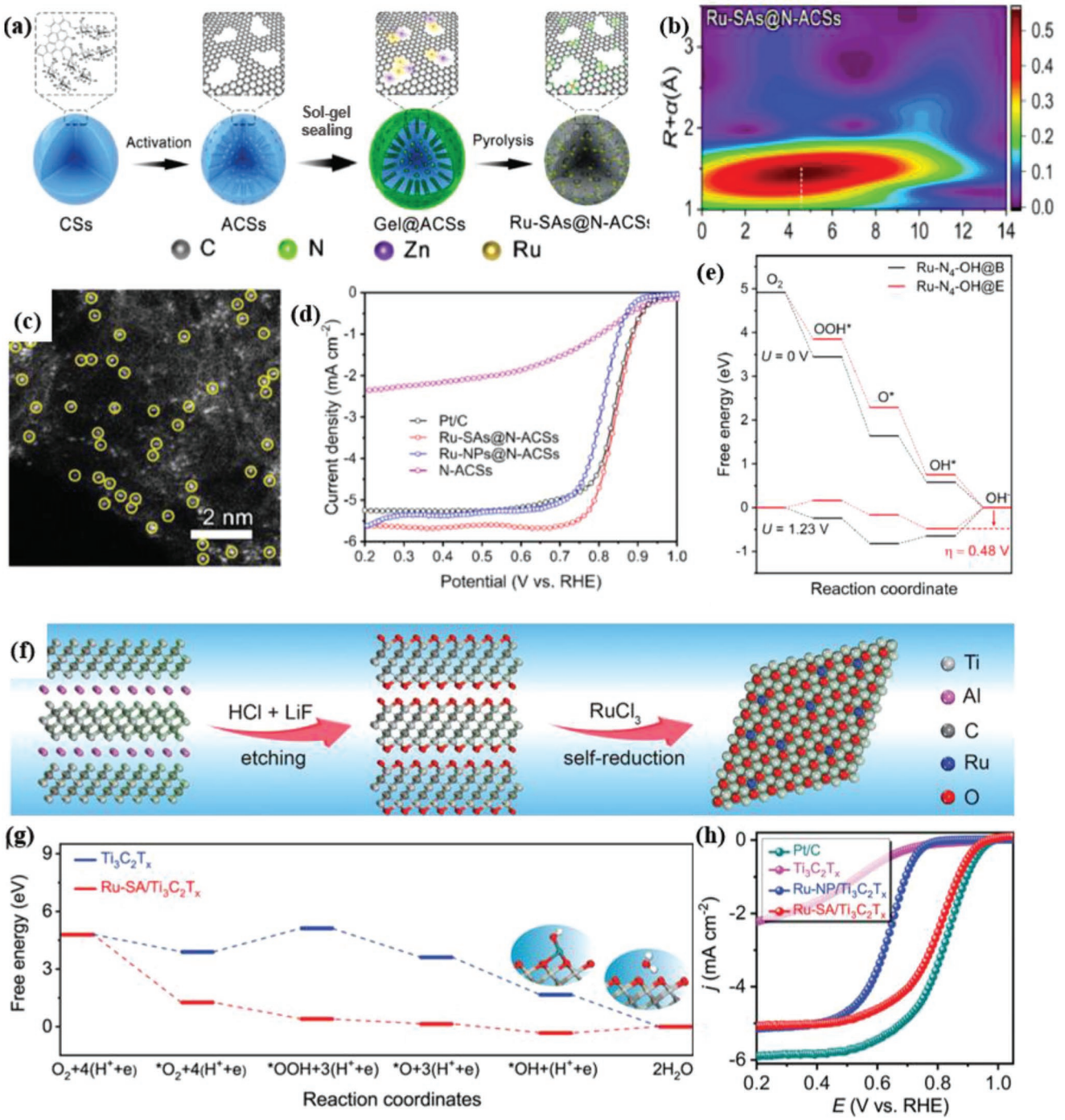

Figure 15. Size engineering strategies of Ru-based catalysts for ORR: a) Synthesis illustration of Ru-SA@N-ACSs electrocatalyst. b) The Ru K-edge wavelet-transforming (WT)–EXAFS plot, and c) HAADF-STEM image of Ru-SAs@N-ACSs. d) ORR polarization curve. e) Gibbs free energy diagrams of Ru-N_4-OH@B and Ru-N_4-OH@E during the ORR reaction at electrode potentials of $U = 1.23$ V and $U = 0$ V (vs RHE). Reproduced with permission.[156] Copyright 2021, Elsevier. f) Schematic diagram of the synthetic route of Ru-SA/$Ti_3C_2T_x$ SACs. g) Free energy changes of relevant intermediates during the ORR process. h) ORR polarization curve. Reproduced with permission.[157] Copyright 2021, Elsevier.

(LOM).[163] Under acidic OER conditions, the dissolution of RuO_2 accelerates and the activity degrades due to the influence of weakly bound lattice O, which is not conducive to OER. Therefore, the engineered Ru-based metal oxides are intensively studied as stable OER electrocatalysts. Designing defect structures can increase the covalent effect of Ru—O and inhibit the dissolution of RuO_2. Furthermore, by introducing an additional metal element into RuO_2 to form M—O—Ru bonds, the lattice O can be stabilized, thereby suppressing LOM and enabling AEM kinetics.[164,165] In the other Ru-based nanomaterials,

Table 2. The engineered Ru-based electrocatalysts for ORR.

Catalysts	Modification strategy	Loading [mg cm^{-2}]	Electrolytes	$E_{1/2}$ [V vs RHE]	Tafel slope [mV dec^{-1}]	Ref.
PdAuRu NSAs	Metal element	–	0.1 M KOH	0.8935	55.31	[151]
RuFe@NC-900	Metal element	0.7 ± 0.1	0.1 M KOH	0.85	140	[152]
Ru-Pt_3Co	Metal element	0.05	0.1 M $HClO_4$	≈0.89	–	[9]
RuN_2 monolayer	Non-metal element	–	–	0.93	–	[153]
Mn-RuO_2	Bimetallic oxides	–	0.1 M KOH	0.86	38.9	[155]
Ru-SA@N-ACSs	Size	0.255	0.1 M KOH	0.86	78	[156]
Ru-SA/$Ti_3C_2T_x$	Size	0.23 wt%	0.1 M $HClO_4$	0.80	27.7	[157]
RuO_x-on-Pd NSs	Heterostructure	–	0.1 M KOH	0.93	35.5	[158]

the size or heterostructure engineering strategies can optimize the desired d-band center through electronic modulation, reduce the reaction energy of the rate-limiting step, and further strengthen the OER pathways.

4.4.1. Surface Structure and Metal Element-Engineered Ru-Based Electrocatalysts for OER

The 2D sheet-like structure composed of interconnected nanocrystals has a large specific surface area and more active sites. The snowflake-like RuCu nanosheets with abundant channels on carbon black (RuCu NSs/C) have been investigated as OER catalysts. The RuCu NSs/C achieved low overpotential at a current density of 10 mA cm^{-2} in acidic and alkane solutions of different concentrations ($\eta_{1\ M\ KOH}$ = 234 mV, $\eta_{0.1\ M\ KOH}$ = 276 mV, $\eta_{0.5\ M\ H2SO4}$ = 236 mV, $\eta_{0.05\ M\ H2SO4}$ = 240 mV). The DFT calculations demonstrated that the induced lattice distortion around the channel structure and the charge transfer between Ru and Cu lowered the reaction energy barriers of RuCu NSs/C for both acidic and basic OER.[166]

4.4.2. Bimetallic Oxides-Engineered Ru-Based Electrocatalysts for OER

Although RuO_2 is regarded as a benchmark catalyst for OER, it is prone to be dissolved and lost stability at higher operating voltages. The incorporation of noble metals, such as Pt, to RuO_2 can significantly increase the OER activity and stability, due to the partial replacement of the Ru atoms leading to the charge redistribution and movement of 4d electron orbital to the Fermi level. The derived single-site Pt-doped RuO_2 hollow nanospheres (SS Pt-RuO_2 HNSs) maintained 100 h without degradation in acidic water splitting (**Figure 16**a–f).[167] Moreover, the incorporation of Pb with pseudocapacitive properties into Ru oxide ($RuPbO_x$) can also optimize the total charge on the $RuPbO_x$ surface (eight to 15 times higher than RuO_2) and thereby facilitate the deprotonation of OOH* and stabilize the intermediates. The OER overpotential (η_{10}) of $RuPbO_x$ is only 191 mV under acidic conditions (Figure 16g–i).[168] CrO_2 is almost inactive for OER, however, Cr can be incorporated into RuO_2 to achieve the boosted OER activity. The bimetallic oxide electrocatalysts $Cr_{0.6}Ru_{0.4}O_2$ with the Cr engineering RuO_2 exhibited altered electronic state, shortened Ru—O bond length, and shifted O p-band center closer to the Fermi level, which is beneficial to the OER process. The as-prepared $Cr_{0.6}Ru_{0.4}O_2$ showed a low overpotential of only 178 mV for the current density of 10 mA cm^{-2} in 0.5 M H_2SO_4, which is much lower than those of commercial RuO_2 (η_{10} = 240 mV) and CrO_2 (almost no OER catalytic activity). Furthermore, due to the less Fermi level occupation of $Cr_{0.6}Ru_{0.4}O_2$, it maintained excellent durability in 10 000 CV cycles and 10 h stability tests.[169] Pyrochlore-type Ru-based bimetallic oxides with fast charge transfer capability are also commonly used for OER. A-site Y^{3+} metal ion partially replaced B-site Ru^{4+} forming yttrium ruthenate pyrochlore metal oxide ($Y_2[Ru_{1.6}Y_{0.4}]O_{7-\delta}$). This uncommon substitution strategy enables Ru to exist in mixed oxidation states of +4 and ±5 and generates oxygen vacancies to maintain the charge neutrality of $Y_2[Ru_{1.6}Y_{0.4}]O_{7-\delta}$, which is beneficial to strengthen the covalent between Ru and O atoms to promote OER process. In 0.1 M $HClO_4$, $Y_2[Ru_{1.6}Y_{0.4}]O_{7-\delta}$ exhibited an onset potential of 1.42 V vs RHE and a Tafel slope of 37 mV dec^{-1}, which is superior to that of the commercial RuO_2 with an onset potential of 1.47 V vs RHE and Tafel slope of 60 mV dec^{-1}.[170]

4.4.3. Size-Engineered Ru-Based Electrocatalysts for OER

It has been reported that atomically dispersed Ru-M dual-sites on carbon supports show excellent OER catalytic performance due to the regulated electronic structure and optimized d-band center. For example, N-doped carbon materials-supported Ru/Co dual-sites catalyst (Ru/Co-N-C) with RuN_4 and CoN_4 atomic centers were obtained by high-temperature pyrolysis and acid etching of self-assembled $RuCl_3/CoCl_2$-UiO-66-NH_2.[171] It is shown that CoN_4 plays the role of regulating the electronic structure of Ru, promoting the covalent interaction of Ru—O, and leading the RuN_4 as the main active center, which highly boosts the OER process. The dual-site Ru/Co-N-C catalyst exhibited excellent OER performance in both acidic and alkaline electrolytes ($\eta_{10,\ acid}$ = 232 mV, $\eta_{10,\ alkaline}$ = 276 mV), which is much superior compared to the single counterparts Ru-N-C ($\eta_{10,\ acid}$ = 297 mV, $\eta_{10,\ alkaline}$ = 347 mV) and commercial RuO_2 ($\eta_{10,\ acid}$ = 329 mV, $\eta_{10,\ alkaline}$ = 379 mV). The alloy substrate, $PtCu_x$/Pt with core–shell structure, is also promising to optimize the catalytic properties of atomically dispersed Ru atoms. Affected by lattice mismatch, the Pt_3Cu core in Ru_1-Pt_3Cu exhibits the largest compressive strain to the Pt shell, which

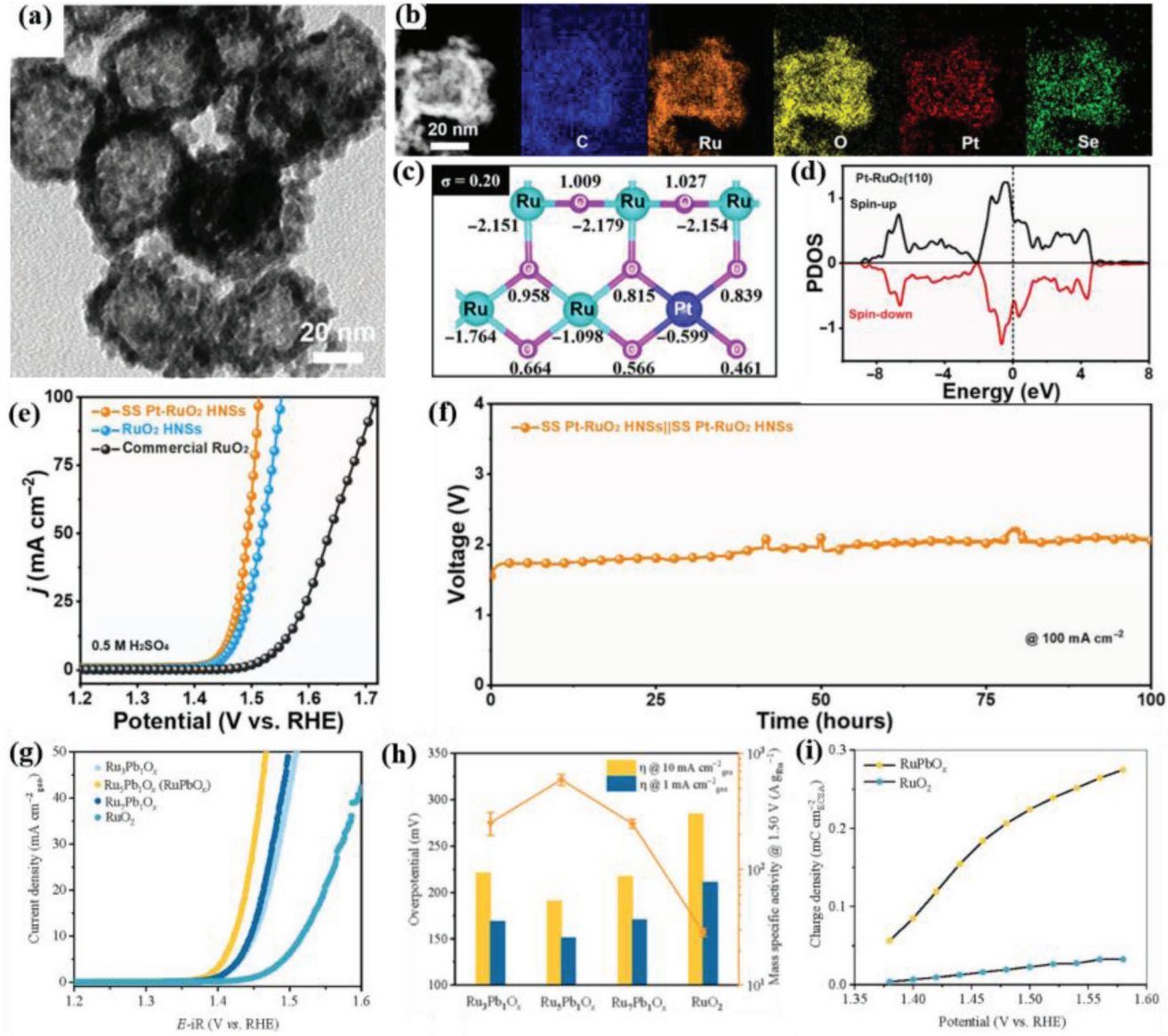

Figure 16. Ru-based bimetallic oxides of Ru-based catalysts for OER: a) TEM image and b) STEM image and STEM-EDS elemental mapping images of SS Pt-RuO_2 HNSs. c) Bader charge numbers of atoms in Pt-RuO_2 (negative values indicate loss of electrons, while positive values indicate gain of electrons) and d) PDOS of 4d orbitals of surface Ru atoms. e) OER polarization curve. f) Chronopotentiometry test of a two-electrode electrolyzer assembled from SS Pt-RuO_2 HNSs. Reproduced with permission.[167] Copyright 2022, American Association for the Advancement of Science. g) OER polarization curves and h) comparison of overpotential and MA for $RuPbO_x$ and control samples. i) Cathodic pulse voltammetry (PV) measurement curve. Reproduced with permission.[168] Copyright 2022, Elsevier.

effectively modulates the electronic structure of the monodispersed Ru single atoms, leading to a low overpotential of η_{10} = 220 mV in 0.1 M $HClO_4$. In situ attenuated total reflection infrared found that the OER catalytic mechanism of Ru_1-Pt_3Cu changed from lattice OER mechanism to an AEM, highly enhancing the catalytic stability to 3000 cycles.[172]

4.4.4. Heterostructure-Engineered Ru-Based Electrocatalysts for OER

In recent years, the hybridization of Ru with nonmetal atoms is often accompanied by the formation of heterostructure to synergistically boost the OER process. The charge redistribution that occurs at the interface of the heterostructure may result in electron-deficient Ru atoms as active centers for the OER, which have a moderate adsorption effect on the O* intermediate, thereby increasing the electrocatalytic activity. Ru/RuS_2 with nonheteroatoms and heterostructure was obtained by using ruthenium oxide (RuO_2) as the Ru source and potassium sulfide (K_2S) as the S source in a eutectic salt system through simultaneous reduction and sulfurization (**Figure 17**a). A distinct heteroplane of Ru and RuS_2 was observed between the Ru/RuS_2 stacked nanosheets (Figure 17b). Ru/RuS_2 delivered a current density of 10 mA cm^{-2} at the overpotential of 201 mV

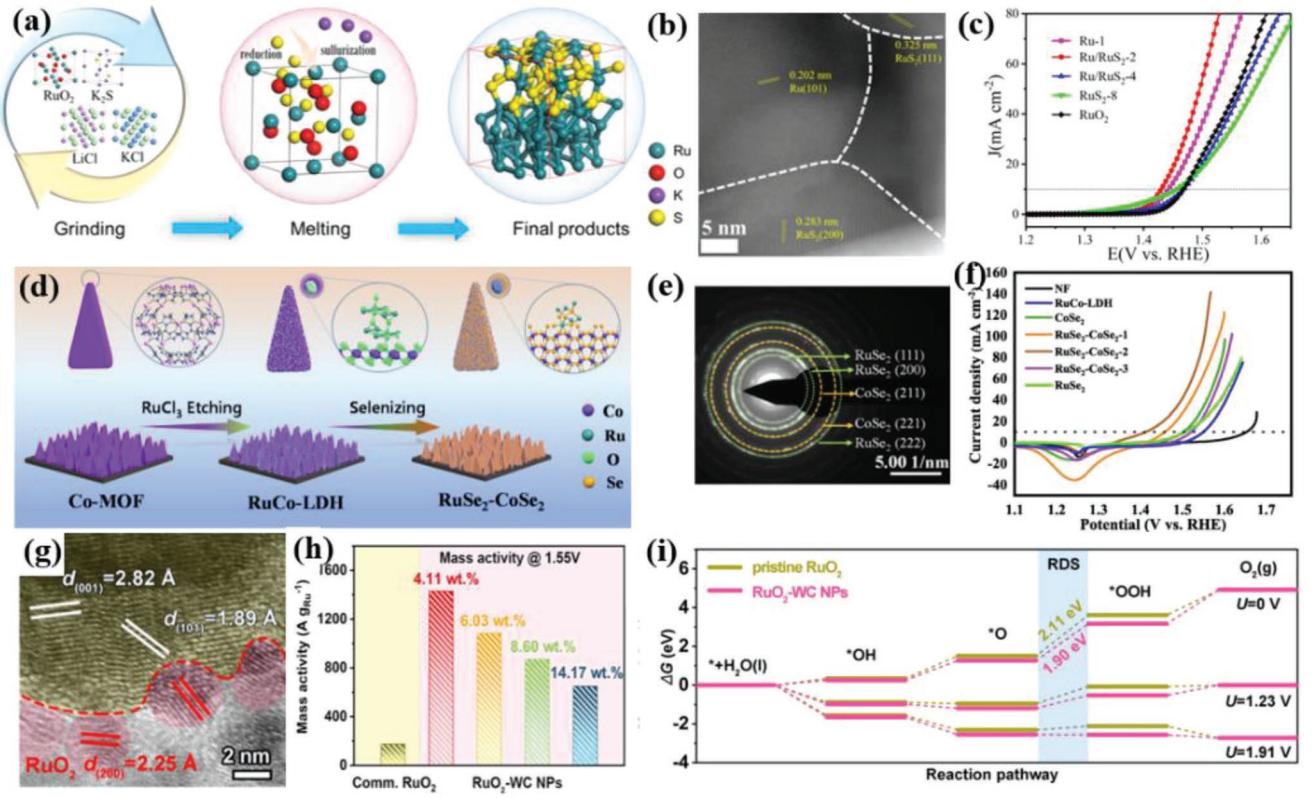

Figure 17. Heterostructure engineering strategies of Ru-based catalysts for OER: a) Schematic illustration of the preparation process of Ru/RuS_2 heterostructure. b) Spherical aberration-corrected scanning transmission electron microscope (ac-STEM) image of RuS_2-Ru. c) OER polarization curves in acidic electrolytes. Reproduced with permission.[173] Copyright 2021, Wiley-VCH. d) Schematic illustration of the preparation process of $RuSe_2$-$CoSe_2$. e) Selected area electron diffraction pattern of $RuSe_2$-$CoSe_2$. f) OER polarization curves of $RuSe_2$-$CoSe_2$ and other reference samples in alkaline electrolyte. Reproduced with permission.[174] Copyright 2022, Elsevier. g) HR-TEM image of RuO_2-WC NPs/CP. h) MA at 1.55 V (vs RHE) in 0.5 M H_2SO_4. i) Free energy diagram of RuO_2-WC NPs and RuO_2 at zero potential, equilibrium potential, and operating potential ($U = 0$, 1.23, and 1.91 V, respectively). Reproduced with permission.[175] Copyright 2022, Wiley-VCH.

for OER in acidic conditions (Figure 17c).[173] A similar heterostructure of $RuSe_2$-$CoSe_2$ was achieved by a combination of ion exchange and low-temperature selenization (Figure 17d,e). The heterostructure played an important role in inhibiting the dissolution of Ru during the OER process. Moreover, the strong interaction between Ru and Co atoms induced optimized electronic structure and O adsorption capacity, resulting in an overpotential of only 200 mV at a current density of 10 mA cm^{-2} (Figure 17f).[174] The WC belonging to transition metal carbide (TMC) has a Pt-like electronic structure around the E_F. Combining it with RuO_2 to form a heterostructure material (RuO_2-WC NPs) further improves the OER activity (Figure 17g). In 0.5 M H_2SO_4 solution, RuO_2-WC NPs exhibited excellent mass activity of 1430 A g_{Ru}^{-1} toward OER, which is eight times over that of commercial RuO_2 (Figure 17h). The DFT calculations demonstrated that WC and RuO_2 are lattice-matched, which facilitates the electrons transfer from WC to RuO_2 at the heterointerface, optimizing the electronic structure of Ru and decreasing the reaction energy barrier of the active intermediate OOH*. In addition, the presence of WC inhibited the over-oxidation of Ru active sites, thereby enhancing the OER stability (Figure 17i).[175] **Table 3** summarizes the OER activity of various Ru-based electrocatalysts.

5. Summary and Outlook

Ru-based catalysts, as the most promising alternative for Pt-based catalysts, have emerged and accelerated many catalytic reactions. In this review, modification strategies for Ru-based nanomaterials have been discussed, which significantly influence the structural and electronic properties. The exposed facets, morphologies, Ru-metal/nonmetal bonds, size effect, heterointerface, etc., induce electronic modulation effects by the intramolecular and intermolecular of the Ru-based nanomaterials, exposing more active sites and resulting in charge redistribution, which optimize the adsorption of reactants/intermediates and catalytic performance. The application progress of engineered Ru-based nanomaterials for hydrogen/oxygen conversion reactions (HER, HOR, ORR, OER) has been summarized, and the relationships between engineering strategies, reaction pathways, and catalytic activity are well-developed. Despite the progress achieved for the engineered Ru-based catalysts, there are still some challenges and opportunities should be focused on the following aspects:

1) Versatile and multifunctional Ru-based catalysts should be established. Ru-based nanomaterials exhibited excellent catalytic ability for HER, HOR, ORR, or OER. In recent years,

Table 3. The engineered Ru-based electrocatalysts for OER.

Catalysts	Modification strategy	Loading [mg cm^{-2}]	Electrolytes	η_{10} [mV vs RHE]	Tafel slope [mV dec^{-1}]	Ref.
RuCu NSs/C	Surface+Metal element	–	1.0 M KOH	234	41.2	[166]
			0.1 M KOH	276	72.9	
			0.5 M H_2SO_4	236	40.4	
			0.05 M H_2SO_4	240	51.4	
SS Pt-RuO_2 HNSs	Bimetallic oxides	0.306	0.5 M H_2SO_4	228	51.0	[167]
$RuPbO_x$	Bimetallic oxides	0.32	0.5 M H_2SO_4	191	39	[168]
$Cr_{0.6}Ru_{0.4}O_2$	Bimetallic oxides	–	0.5 M H_2SO_4	178	58	[169]
$Y_2[Ru_{1.6}Y_{0.4}]O_{7-\delta}$	Bimetallic oxides	–	0.1 M $HClO_4$	–	37	[170]
Ru/Co-N-C	Size	0.4	1.0 M KOH	276	27.8	[171]
			0.5 M H_2SO_4	232	23.3	
Ru_1-Pt_3Cu	Size+Heterostructure	0.00192	0.1 M $HClO_4$	220	–	[172]
Ru/RuS_2	Heterostructure	0.849	0.5 M H_2SO_4	201	47.2	[173]
$RuSe_2$-$CoSe_2$	Heterostructure	–	1.0 M KOH	200	53.2	[174]
RuO_2-WC NPs	Heterostructure	4.11 wt%	0.5 M H_2SO_4	347	88.5	[175]

the development of versatile and multifunctional catalysts is crucial for the advanced green processes and sustainable chemistry in the industry. There is still some gap between the catalytic activity of these Ru-based electrocatalysts and specialized catalysts in terms of catalytic performance. Therefore, a multiactive-site strategy can be adopted to combine the active components for different catalytic reactions to design Ru-based composites. And combining components or phase structures with different catalytic roles to construct heterostructure promotes multifunctional catalysis with synergistic effects.

2) Much-needed improved stability. After unremitting efforts devoted, many Ru-based catalysts with advanced nanostructures have shown excellent electrocatalytic performance. However, under the highly corrosive, high temperature or high potential reaction conditions, the dissolution of Ru-based nanomaterials reduces the stability of the catalyst, which seriously hinders its industrial application. Therefore, it is of great significance to strive to develop Ru-based electrocatalysts with high catalytic activity and stability under the conditions of industrial application.
3) Advanced characterization technology. For heterogenous electrocatalytic reactions, the surface of the catalyst is an important site for the catalytic reaction. The interaction between the active sites on the surface and the active intermediates is the key factor affecting the catalytic activity. Therefore, it is necessary to use more advanced in situ characterization techniques, such as in situ Raman, Fourier transform infrared spectroscopy (in situ FTIR), and X-ray absorption spectroscopy (in situ XAS), to identify the changes of the active sites, and the binding states between the active sites and intermediates during the electrocatalytic reactions occurring on Ru-based electrocatalysts.
4) Comprehensive and advanced theoretical calculation. Although the theoretical calculations have been used to study the reaction mechanism of Ru-based nanomaterials, most of these computational results are ignoring the real experimental conditions. Therefore, closely linking the DFT calculations with the experimental results, especially the in situ characterization results, will better reveal the real electrocatalytic process of Ru-based catalysts. Moreover, theoretical calculation is also promising to screen the element to be incorporated or specific atomic structure of Ru-based materials for targeted catalytic activity and stability.
5) Shorten the gap between experimental research and industrial applications. Currently, significant progress has been made in the research and application of Ru-based materials for hydrogen/oxygen conversion reactions. However, how to large-scale apply Ru-based electrocatalysts to practical applications is still a huge challenge. Small batch preparation and controllable experimental conditions provide great convenience for the development of academic research, whereas more critical, such as ensuring equipment stability, process repeatability, and scale-up experiments, are needed for industrial production. Even though Ru-based catalysts have made considerable progress in the practical application of dimensionally stable anode and some organically catalyzed reactions such as asymmetric hydrogenation reactions, there is still a long way to go before larger-scale commercial applications. Therefore, finding a way to reduce the gap between experimental research and industrial application is an urgent challenge for Ru-based catalysts.

Acknowledgements

H.L. acknowledges the supported by the Australian Research Council (ARC) through the Discovery Project (DP180102297), Future Fellow Project (FT180100705). J.H. thanks the support from Open Project of State Key Laboratory of Advanced Special Steel, Shanghai Key Laboratory of Advanced Ferrometallurgy, Shanghai University (SKLASS 2021-**). All authors thank the support from "Joint International Laboratory on Environmental and Energy Frontier Materials" and "Innovation Research Team of High-Level Local Universities in Shanghai."

Open access publishing facilitated by University of Technology Sydney, as part of the Wiley - University of Technology Sydney agreement via the Council of Australian University Librarians.

Conflict of Interest

The authors declare no conflict of interest.

Keywords

energy conversion reactions, engineering strategies, induced effects, Ru-based materials

Received: June 22, 2022
Revised: August 10, 2022
Published online: September 1, 2022

[1] C. Zou, Q. Zhao, G. Zhang, B. Xiong, *Nat. Gas Ind. B* **2016**, *3*, 1.
[2] A. G. Olabi, M. A. Abdelkareem, *Renewable Sustainable Energy Rev.* **2022**, *158*, 112111.
[3] R. Schlögl, *Green Chem.* **2021**, *23*, 1584.
[4] S. Keleş, *Energy Sources, Part A* **2011**, *33*, 1184.
[5] S. Chu, Y. Cui, N. Liu, *Nat. Mater.* **2017**, *16*, 16.
[6] F. Dawood, M. Anda, G. M. Shafiullah, *Int. J. Hydrogen Energy* **2020**, *45*, 3847.
[7] A. T. John, *Science* **2004**, *305*, 972.
[8] S. Mekhilef, R. Saidur, A. Safari, *Renewable Sustainable Energy Rev.* **2012**, *16*, 981.
[9] Y. Zhu, J. Peng, X. Zhu, L. Bu, Q. Shao, C. W. Pao, Z. Hu, Y. Li, J. Wu, X. Huang, *Nano Lett.* **2021**, *21*, 6625.
[10] S. Zaman, L. Huang, A. I. Douka, H. Yang, B. You, B. Y. Xia, *Angew. Chem., Int. Ed.* **2021**, *60*, 17832.
[11] O. Z. Sharaf, M. F. Orhan, *Renewable Sustainable Energy Rev.* **2014**, *32*, 810.
[12] L. Zhang, K. Doyle-Davis, X. Sun, *Energy Environ. Sci.* **2019**, *12*, 492.
[13] X. Wang, L. Zhao, X. Li, Y. Liu, Y. Wang, Q. Yao, J. Xie, Q. Xue, Z. Yan, X. Yuan, W. Xing, *Nat. Commun.* **2022**, *13*, 1596.
[14] F. Xu, S. Cai, B. Lin, L. Yang, H. Le, S. Mu, *Small* **2022**, *18*, 2107387.
[15] Z. Zhang, H. Liu, L. Ni, Z.-L. Zhao, H. Li, *J. Energy Chem.* **2022**, *72*, 176.
[16] Y. Xue, L. Shi, X. Liu, J. Fang, X. Wang, B. P. Setzler, W. Zhu, Y. Yan, Z. Zhuang, *Nat. Commun.* **2020**, *11*, 5651.
[17] W. R. Crowell, D. M. Yost, J. M. Carter, *J. Am. Chem. Soc.* **1929**, *51*, 786.
[18] F. Gortsema, J. Cobble, *J. Am. Chem. Soc.* **1959**, *81*, 5516.
[19] N. Danilovic, R. Subbaraman, K.-C. Chang, S. H. Chang, Y. J. Kang, J. Snyder, A. P. Paulikas, D. Strmcnik, Y.-T. Kim, D. Myers, V. R. Stamenkovic, N. M. Markovic, *J. Phys. Chem. Lett.* **2014**, *5*, 2474.
[20] R. Frydendal, E. A. Paoli, B. P. Knudsen, B. Wickman, P. Malacrida, I. E. L. Stephens, I. Chorkendorff, *ChemElectroChem* **2014**, *1*, 2075.
[21] N. R. Elezović, B. M. Babić, V. R. Radmilović, N. V. Krstajić, *J. Electrochem. Soc.* **2013**, *160*, F1151.
[22] H. Tributsch, *J. Photochem.* **1985**, *29*, 89.
[23] L. Liu, J.-W. Lee, B. N. Popov, *J. Power Sources* **2006**, *162*, 1099.
[24] C. M. Johnston, D. Cao, J.-H. Choi, P. K. Babu, F. Garzon, P. Zelenay, *J. Electroanal. Chem.* **2011**, *662*, 257.
[25] M. Watanabe, S. Motoo, *J. Electroanal. Chem. Interfacial Electrochem.* **1975**, *60*, 275.
[26] P. K. Babu, A. Lewera, J. H. Chung, R. Hunger, W. Jaegermann, N. Alonso-Vante, A. Wieckowski, E. Oldfield, *J. Am. Chem. Soc.* **2007**, *129*, 15140.
[27] L. Colmenares, Z. Jusys, R. J. Behm, *Langmuir* **2006**, *22*, 10437.
[28] C. Zhang, J. Sha, H. Fei, M. Liu, S. Yazdi, J. Zhang, Q. Zhong, X. Zou, N. Zhao, H. Yu, Z. Jiang, E. Ringe, B. I. Yakobson, J. Dong, D. Chen, J. M. Tour, *ACS Nano* **2017**, *11*, 6930.
[29] Y. Li, L. A. Zhang, Y. Qin, F. Chu, Y. Kong, Y. Tao, Y. Li, Y. Bu, D. Ding, M. Liu, *ACS Catal.* **2018**, *8*, 5714.
[30] M. Zhao, Y. Xia, *Nat. Rev. Mater.* **2020**, *5*, 440.
[31] J. Creus, J. De Tovar, N. Romero, J. Garcia-Anton, K. Philippot, R. Bofill, X. Sala, *ChemSusChem* **2019**, *12*, 2493.
[32] F. Zhou, L. Zhang, J. Li, Q. Wang, Y. Chen, H. Chen, G. Lu, G. Chen, H. Jin, J. Wang, *Eng. Rep.* **2021**, *3*, 12437.
[33] H. Sun, W. Jung, *J. Mater. Chem. A* **2021**, *9*, 15506.
[34] W. Luo, Y. Wang, C. Cheng, *Mater. Today Phys.* **2020**, *15*, 100274.
[35] J. Yu, Q. He, G. Yang, W. Zhou, Z. Shao, M. Ni, *ACS Catal.* **2019**, *9*, 9973.
[36] L. S. Kumara, O. Sakata, S. Kohara, A. Yang, C. Song, K. Kusada, H. Kobayashi, H. Kitagawa, *Phys. Chem. Chem. Phys.* **2016**, *18*, 30622.
[37] S. H. Joo, J. Y. Park, J. R. Renzas, D. R. Butcher, W. Huang, G. A. Somorjai, *Nano Lett.* **2010**, *10*, 2709.
[38] M. Zhao, Z. D. Hood, M. Vara, K. D. Gilroy, M. Chi, Y. Xia, *ACS Nano* **2019**, *13*, 7241.
[39] X. Kong, K. Xu, C. Zhang, J. Dai, S. Norooz Oliaee, L. Li, X. Zeng, C. Wu, Z. Peng, *ACS Catal.* **2016**, *6*, 1487.
[40] K. Kusada, H. Kobayashi, T. Yamamoto, S. Matsumura, N. Sumi, K. Sato, K. Nagaoka, Y. Kubota, H. Kitagawa, *J. Am. Chem. Soc.* **2013**, *135*, 5493.
[41] M. Zhao, L. Figueroa-Cosme, A. O. Elnabawy, M. Vara, X. Yang, L. T. Roling, M. Chi, M. Mavrikakis, Y. Xia, *Nano Lett.* **2016**, *16*, 5310.
[42] Y. Zheng, Y. Jiao, Y. Zhu, L. H. Li, Y. Han, Y. Chen, M. Jaroniec, S. Z. Qiao, *J. Am. Chem. Soc.* **2016**, *138*, 16174.
[43] T. Zhao, D. Xiao, Y. Chen, X. Tang, M. Gong, S. Deng, X. Liu, J. Ma, X. Zhao, D. Wang, *J. Energy Chem.* **2021**, *61*, 15.
[44] K. Gao, Y. Wang, Z. Wang, Z. Zhu, J. Wang, Z. Luo, C. Zhang, X. Huang, H. Zhang, W. Huang, *Chem. Commun.* **2018**, *54*, 4613.
[45] M. Zhao, Z. Chen, Z. Lyu, Z. D. Hood, M. Xie, M. Vara, M. Chi, Y. Xia, *J. Am. Chem. Soc.* **2019**, *141*, 7028.
[46] A. R. Poerwoprajitno, L. Gloag, T. M. Benedetti, S. Cheong, J. Watt, D. L. Huber, J. J. Gooding, R. D. Tilley, *Small* **2019**, *15*, 1804577.
[47] M. Escudero-Escribano, K. D. Jensen, A. W. Jensen, *Curr. Opin. Electrochem.* **2018**, *8*, 135.
[48] Q. Xue, Y. Zhao, J. Zhu, Y. Ding, T. Wang, H. Sun, F. Li, P. Chen, P. Jin, S. Yin, Y. Chen, *J. Mater. Chem. A* **2021**, *9*, 8444.
[49] J. Zhang, X. Qu, Y. Han, L. Shen, S. Yin, G. Li, Y. Jiang, S. Sun, *Appl. Catal., B* **2020**, *263*, 118345.
[50] K. Li, Y. Li, Y. Wang, J. Ge, C. Liu, W. Xing, *Energy Environ. Sci.* **2018**, *11*, 1232.
[51] S. Zhu, X. Qin, F. Xiao, S. Yang, Y. Xu, Z. Tan, J. Li, J. Yan, Q. Chen, M. Chen, M. Shao, *Nat. Catal.* **2021**, *4*, 711.
[52] D. Strmcnik, M. Uchimura, C. Wang, R. Subbaraman, N. Danilovic, D. van der Vliet, A. P. Paulikas, V. R. Stamenkovic, N. M. Markovic, *Nat. Commun.* **2013**, *5*, 300.
[53] Y. Wang, G. Wang, G. Li, B. Huang, J. Pan, Q. Liu, J. Han, L. Xiao, J. Lu, L. Zhuang, *Energy Environ. Sci.* **2015**, *8*, 177.
[54] D. Wu, K. Kusada, S. Yoshioka, T. Yamamoto, T. Toriyama, S. Matsumura, Y. Chen, O. Seo, J. Kim, C. Song, S. Hiroi, O. Sakata, T. Ina, S. Kawaguchi, Y. Kubota, H. Kobayashi, H. Kitagawa, *Nat. Commun.* **2021**, *12*, 1145.
[55] D. Zhang, H. Zhao, B. Huang, B. Li, H. Li, Y. Han, Z. Wang, X. Wu, Y. Pan, Y. Sun, X. Sun, J. Lai, L. Wang, *ACS Cent. Sci.* **2019**, *5*, 1991.
[56] Q. Wu, M. Luo, J. Han, W. Peng, Y. Zhao, D. Chen, M. Peng, J. Liu, F. M. F. de Groot, Y. Tan, *ACS Energy Lett.* **2019**, *5*, 192.
[57] K. Shah, R. Dai, M. Mateen, Z. Hassan, Z. Zhuang, C. Liu, M. Israr, W. C. Cheong, B. Hu, R. Tu, C. Zhang, X. Chen, Q. Peng, C. Chen, Y. Li, *Angew. Chem., Int. Ed.* **2022**, *134*, 202114951.
[58] D. Chen, R. Lu, Z. Pu, J. Zhu, H.-W. Li, F. Liu, S. Hu, X. Luo, J. Wu, Y. Zhao, S. Mu, *Appl. Catal., B* **2020**, *279*, 119396.
[59] G. Liu, W. Zhou, B. Chen, Q. Zhang, X. Cui, B. Li, Z. Lai, Y. Chen, Z. Zhang, L. Gu, H. Zhang, *Nano Energy* **2019**, *66*, 104173.
[60] Z. Zhang, P. Li, Q. Wang, Q. Feng, *J. Mater. Chem. A* **2019**, *7*, 2780.
[61] Y. Zhao, D. Wu, W. Luo, *ACS Sustainable Chem. Eng.* **2022**, *10*, 1616.
[62] Z. Li, X. Lu, J. Teng, Y. Zhou, W. Zhuang, *Nanoscale* **2021**, *13*, 11314.
[63] W. Luo, Y. Wang, X. Li, C. Cheng, *Nanotechnology* **2020**, *31*, 295401.
[64] R. R. Rao, M. J. Kolb, N. B. Halck, A. F. Pedersen, A. Mehta, H. You, K. A. Stoerzinger, Z. Feng, H. A. Hansen, H. Zhou, L. Giordano,

J. Rossmeisl, T. Vegge, I. Chorkendorff, I. E. L. Stephens, Y. Shao-Horn, *Energy Environ. Sci.* **2017**, *10*, 2626.
[65] C. Roy, R. R. Rao, K. A. Stoerzinger, J. Hwang, J. Rossmeisl, I. Chorkendorff, Y. Shao-Horn, I. E. L. Stephens, *ACS Energy Lett.* **2018**, *3*, 2045.
[66] K. A. Stoerzinger, R. R. Rao, X. R. Wang, W. T. Hong, C. M. Rouleau, Y. Shao-Horn, *Chem* **2017**, *2*, 668.
[67] B. Hammer, O. H. Nielsen, J. K. Nrskov, *Catal. Lett.* **1997**, *46*, 31.
[68] G. Wu, X. Zheng, P. Cui, H. Jiang, X. Wang, Y. Qu, W. Chen, Y. Lin, H. Li, X. Han, Y. Hu, P. Liu, Q. Zhang, J. Ge, Y. Yao, R. Sun, Y. Wu, L. Gu, X. Hong, Y. Li, *Nat. Commun.* **2019**, *10*, 4855.
[69] E. Tsuji, A. Imanishi, K.-I. Fukui, Y. Nakato, *Electrochim. Acta* **2011**, *56*, 2009.
[70] L. Zhang, H. Jang, H. Liu, M. G. Kim, D. Yang, S. Liu, X. Liu, J. Cho, *Angew. Chem., Int. Ed.* **2021**, *60*, 18821.
[71] H. Chen, B. Zhang, X. Liang, X. Zou, *Chin. J. Catal.* **2022**, *43*, 611.
[72] Y. Yang, Y. Yu, J. Li, Q. Chen, Y. Du, P. Rao, R. Li, C. Jia, Z. Kang, P. Deng, Y. Shen, X. Tian, *Nano-Micro Lett.* **2021**, *13*, 160.
[73] Y. Zhao, X. Wang, G. Cheng, W. Luo, *ACS Catal.* **2020**, *10*, 11751.
[74] H. Chen, X. Zou, *Inorg. Chem. Front.* **2020**, *7*, 2248.
[75] X. Ai, X. Zou, H. Chen, Y. Su, X. Feng, Q. Li, Y. Liu, Y. Zhang, X. Zou, *Angew. Chem., Int. Ed.* **2020**, *59*, 3961.
[76] J. Su, R. Ge, K. Jiang, Y. Dong, F. Hao, Z. Tian, G. Chen, L. Chen, *Adv. Mater.* **2018**, *30*, 1801351.
[77] V. Petrykin, K. Macounova, J. Franc, O. Shlyakhtin, M. Klementova, S. Mukerjee, P. Krtil, *Chem. Mater.* **2011**, *23*, 200.
[78] L.-E. Owe, M. Tsypkin, K. S. Wallwork, R. G. Haverkamp, S. Sunde, *Electrochim. Acta* **2012**, *70*, 158.
[79] J. M. Roller, M. J. Arellano-Jiménez, R. Jain, H. Yu, C. B. Carter, R. Maric, *J. Electrochem. Soc.* **2013**, *160*, F716.
[80] A. Martínez-Séptimo, M. A. Valenzuela, P. Del Angel, R.d.G. González-Huerta, *Int. J. Hydrogen Energy* **2021**, *46*, 25918.
[81] Y. B. Cho, A. Yu, C. Lee, M. H. Kim, Y. Lee, *Adv. Mater. Interfaces* **2018**, *10*, 541.
[82] J. Su, R. Ge, K. Jiang, Y. Dong, F. Hao, Z. Tian, G. Chen, L. Chen, *Adv. Mater.* **2018**, *30*, 1801351.
[83] J. Wang, Y. Ji, R. Yin, Y. Li, Q. Shao, X. Huang, *J. Mater. Chem. A* **2019**, *7*, 6411.
[84] J. Park, M. Risch, G. Nam, M. Park, T. J. Shin, S. Park, M. G. Kim, Y. Shao-Horn, J. Cho, *Energy Environ. Sci.* **2017**, *10*, 129.
[85] H. Horowitz, J. M. Longo, H. Horowitz, *J. Electrochem. Soc.* **1983**, *130*, 1851.
[86] K. T. Lee, B. W. Lee, M. A. Camaratta, E. D. Wachsman, *RSC Adv.* **2013**, *3*, 19866.
[87] J. Kim, P. C. Shih, K. C. Tsao, Y. T. Pan, X. Yin, C. J. Sun, H. Yang, *J. Am. Chem. Soc.* **2017**, *139*, 12076.
[88] W. Li, Y. Liu, M. Wu, X. Feng, S. A. T. Redfern, Y. Shang, X. Yong, T. Feng, K. Wu, Z. Liu, B. Li, Z. Chen, J. S. Tse, S. Lu, B. Yang, *Adv. Mater.* **2018**, *30*, 1800676.
[89] K. Kwak, D. Lee, *Acc. Chem. Res.* **2019**, *52*, 12.
[90] Y. Wang, W. Luo, H. Li, C. Cheng, *Nanoscale Adv.* **2021**, *3*, 5068.
[91] Y. L. Wu, X. Li, Y. S. Wei, Z. Fu, W. Wei, X. T. Wu, Q. L. Zhu, Q. Xu, *Adv. Mater.* **2021**, *33*, 2006965.
[92] J. Guo, J. Huo, Y. Liu, W. Wu, Y. Wang, M. Wu, H. Liu, G. Wang, *Small Methods* **2019**, *3*, 1900159.
[93] H. Tian, A. Song, H. Tian, J. Liu, G. Shao, H. Liu, G. Wang, *Chem. Sci.* **2021**, *12*, 7656.
[94] J. Huo, Z. Shen, X. Cao, L. Li, Y. Zhao, H. Liu, G. Wang, *Small* **2022**, *18*, 2202394.
[95] L. Zhang, R. Si, H. Liu, N. Chen, Q. Wang, K. Adair, Z. Wang, J. Chen, Z. Song, J. Li, M. N. Banis, R. Li, T. K. Sham, M. Gu, L. M. Liu, G. A. Botton, X. Sun, *Nat. Commun.* **2019**, *10*, 4936.
[96] Y. Sun, Z. Xue, Q. Liu, Y. Jia, Y. Li, K. Liu, Y. Lin, M. Liu, G. Li, C. Y. Su, *Nat. Commun.* **2021**, *12*, 1369.
[97] P. Li, M. Wang, X. Duan, L. Zheng, X. Cheng, Y. Zhang, Y. Kuang, Y. Li, Q. Ma, Z. Feng, W. Liu, X. Sun, *Nat. Commun.* **2019**, *10*, 1711.
[98] D. Zhang, H. Miao, X. Wu, Z. Wang, H. Zhao, Y. Shi, X. Chen, Z. Xiao, J. Lai, L. Wang, *Chin. J. Catal.* **2022**, *43*, 1148.
[99] J. Li, M. Hou, Z. Zhang, *Nanoscale* **2022**, *14*, 8096.
[100] Y. Zhu, H. A. Tahini, Y. Wang, Q. Lin, Y. Liang, C. M. Doherty, Y. Liu, X. Li, J. Lu, S. C. Smith, C. Selomulya, X. Zhang, Z. Shao, H. Wang, *J. Mater. Chem. A* **2019**, *7*, 14222.
[101] Y. Zhao, J. Zhang, Y. Xie, B. Sun, J. Jiang, W. J. Jiang, S. Xi, H. Y. Yang, K. Yan, S. Wang, X. Guo, P. Li, Z. Han, X. Lu, H. Liu, G. Wang, *Nano Lett.* **2021**, *21*, 823.
[102] Y. Nanba, T. Ishimoto, M. Koyama, *J. Phys. Chem. C* **2017**, *121*, 27445.
[103] Y. Luo, X. Luo, G. Wu, Z. Li, G. Wang, B. Jiang, Y. Hu, T. Chao, H. Ju, J. Zhu, Z. Zhuang, Y. Wu, X. Hong, Y. Li, *ACS Appl. Mater. Interfaces* **2018**, *10*, 34147.
[104] Y. Liu, S. Liu, Y. Wang, Q. Zhang, L. Gu, S. Zhao, D. Xu, Y. Li, J. Bao, Z. Dai, *J. Am. Chem. Soc.* **2018**, *140*, 2731.
[105] Y. Hu, X. Luo, G. Wu, T. Chao, Z. Li, Y. Qu, H. Li, Y. Wu, B. Jiang, X. Hong, *ACS Appl. Mater. Interfaces* **2019**, *11*, 42298.
[106] J. Shan, Y. Zheng, B. Shi, K. Davey, S.-Z. Qiao, *ACS Energy Lett.* **2019**, *4*, 2719.
[107] X. Wang, Y. Zhu, A. Vasileff, Y. Jiao, S. Chen, L. Song, B. Zheng, Y. Zheng, S.-Z. Qiao, *ACS Energy Lett.* **2018**, *3*, 1198.
[108] J. Shan, C. Guo, Y. Zhu, S. Chen, L. Song, M. Jaroniec, Y. Zheng, S.-Z. Qiao, *Chem* **2019**, *5*, 445.
[109] Z. H. Xue, H. Su, Q. Y. Yu, B. Zhang, H. H. Wang, X. H. Li, J. S. Chen, *Adv. Energy Mater.* **2017**, *7*, 1602355.
[110] N. Wang, S. Ning, X. Yu, D. Chen, Z. Li, J. Xu, H. Meng, D. Zhao, L. Li, Q. Liu, B. Lu, S. Chen, *Appl. Catal., B* **2022**, *302*, 120838.
[111] Q. Ju, R. Ma, Y. Pei, B. Guo, Z. Li, Q. Liu, T. Thomas, M. Yang, G. J. Hutchings, J. Wang, *Adv. Energy Mater.* **2020**, *10*, 2000067.
[112] W. Peng, M. Luo, X. Xu, K. Jiang, M. Peng, D. Chen, T. S. Chan, Y. Tan, *Adv. Energy Mater.* **2020**, *10*, 2001364.
[113] S.-Y. Bae, J. Mahmood, I.-Y. Jeon, J.-B. Baek, *Nanoscale Horiz.* **2020**, *5*, 43.
[114] C. Li, J. B. Baek, *ACS Omega* **2020**, *5*, 31.
[115] S. Anantharaj, *Curr. Opin. Electrochem.* **2022**, *33*, 100961.
[116] X. Tian, P. Zhao, W. Sheng, *Adv. Mater.* **2019**, *31*, 1808066.
[117] A. Y. Faid, A. O. Barnett, F. Seland, S. Sunde, *J. Electrochem. Soc.* **2019**, *166*, F519.
[118] Z. W. Seh, J. Kibsgaard, C. F. Dickens, I. Chorkendorff, J. K. Norskov, T. F. Jaramillo, *Science* **2017**, *355*, eaad4998.
[119] Y. Wang, W. Qiu, E. Song, F. Gu, Z. Zheng, X. Zhao, Y. Zhao, J. Liu, W. Zhang, *Natl. Sci. Rev.* **2018**, *5*, 327.
[120] Q. Lu, A. L. Wang, H. Cheng, Y. Gong, Q. Yun, N. Yang, B. Li, B. Chen, Q. Zhang, Y. Zong, L. Gu, H. Zhang, *Small* **2018**, *14*, 1801090.
[121] J. Zhang, X. Mao, S. Wang, L. Liang, M. Cao, L. Wang, G. Li, Y. Xu, X. Huang, *Angew. Chem., Int. Ed.* **2022**, *61*, 202116867.
[122] X. Qin, L. Zhang, G.-L. Xu, S. Zhu, Q. Wang, M. Gu, X. Zhang, C. Sun, P. B. Balbuena, K. Amine, M. Shao, *ACS Catal.* **2019**, *9*, 9614.
[123] C. Cai, K. Liu, Y. Zhu, P. Li, Q. Wang, B. Liu, S. Chen, H. Li, L. Zhu, H. Li, J. Fu, Y. Chen, E. Pensa, J. Hu, Y. R. Lu, T. S. Chan, E. Cortes, M. Liu, *Angew. Chem., Int. Ed.* **2021**, *34*, 202113664.
[124] H. Chen, X. Ai, W. Liu, Z. Xie, W. Feng, W. Chen, X. Zou, *Angew. Chem., Int. Ed.* **2019**, *58*, 11409.
[125] Q. Li, X. Zou, X. Ai, H. Chen, L. Sun, X. Zou, *Adv. Energy Mater.* **2018**, *9*, 1803369.
[126] C. Li, H. Jang, S. Liu, M. G. Kim, L. Hou, X. Liu, J. Cho, *Adv. Energy Mater.* **2022**, *12*, 2200029.
[127] Q. Yao, J. Le, S. Yang, J. Cheng, Q. Shao, X. Huang, *Chin. J. Catal.* **2022**, *43*, 1493.
[128] Y. Wu, R. Yao, Q. Zhao, J. Li, G. Liu, *Chem. Eng. J.* **2022**, *439*, 135699.
[129] C. Xu, M. Ming, Q. Wang, C. Yang, G. Fan, Y. Wang, D. Gao, J. Bi, Y. Zhang, *J. Mater. Chem. A* **2018**, *6*, 14380.

[130] Q. He, D. Tian, H. Jiang, D. Cao, S. Wei, D. Liu, P. Song, Y. Lin, L. Song, *Adv. Mater.* **2020**, *32*, 1906972.
[131] Q. He, Y. Zhou, H. Shou, X. Wang, P. Zhang, W. Xu, S. Qiao, C. Wu, H. Liu, D. Liu, S. Chen, R. Long, Z. Qi, X. Wu, L. Song, *Adv. Mater.* **2022**, *34*, 2110604.
[132] Y. Wei, G. Xu, Y. Wei, L. Ji, T. Wang, Z. Liu, S. Wang, *Sci. China Mater.* **2022**, https://doi.org/10.1007/s40843-022-2001-7.
[133] D. Cao, J. Wang, H. Xu, D. Cheng, *Small* **2020**, *16*, 2000924.
[134] Y. Qiu, X. Xie, W. Li, Y. Shao, *Chin. J. Catal.* **2021**, *42*, 2094.
[135] Y. Li, J. Abbott, Y. Sun, J. Sun, Y. Du, X. Han, G. Wu, P. Xu, *Appl. Catal., B* **2019**, *258*, 117952.
[136] Y. Zhou, Z. Xie, J. Jiang, J. Wang, X. Song, Q. He, W. Ding, Z. Wei, *Nat. Catal.* **2020**, *3*, 454.
[137] B. Qin, H. Yu, X. Gao, D. Yao, X. Sun, W. Song, B. Yi, Z. Shao, *J. Mater. Chem. A* **2018**, *6*, 20374.
[138] J. Mao, C. T. He, J. Pei, Y. Liu, J. Li, W. Chen, D. He, D. Wang, Y. Li, *Nano Lett.* **2020**, *20*, 3442.
[139] Y. Zhao, X. Wang, Z. Li, P. Zhao, C. Tao, G. Cheng, W. Luo, *Chin. Chem. Lett.* **2022**, *33*, 1065.
[140] P. Wang, C. Wang, Y. Yang, S. Chen, Z. Cheng, M. Huang, H. Tong, Q. Chen, *Adv. Mater. Interfaces* **2022**, *9*, 2102193.
[141] J. Wang, J. Liu, B. Zhang, J. Gao, G. Liu, X. Cui, J.-X. Liu, L. Jiang, *J. Mater. Chem. A* **2021**, *9*, 22934.
[142] J. Ohyama, T. Sato, Y. Yamamoto, S. Arai, A. Satsuma, *J. Am. Chem. Soc.* **2013**, *135*, 8016.
[143] Z. Zhang, L. Ni, H. Liu, Z.-L. Zhao, X.-Z. Yuan, H. Li, *Sci. China Chem.* **2022**, *65*, 611.
[144] R. Wang, D. Li, S. Maurya, Y. S. Kim, Y. Wu, Y. Liu, D. Strmcnik, N. M. Markovic, V. R. Stamenkovic, *Nanoscale Horiz.* **2020**, *5*, 316.
[145] B. Xu, Y. Zhang, L. Li, Q. Shao, X. Huang, *Coord. Chem. Rev.* **2022**, *459*, 214388.
[146] Z. Lu, G. Chen, S. Siahrostami, Z. Chen, K. Liu, J. Xie, L. Liao, T. Wu, D. Lin, Y. Liu, *Nat. Catal.* **2018**, *1*, 156.
[147] T. Wang, A. Chutia, D. J. L. Brett, P. R. Shearing, G. He, G. Chai, I. P. Parkin, *Energy Environ. Sci.* **2021**, *14*, 2639.
[148] H. Teller, O. Krichevski, M. Gur, A. Gedanken, A. Schechter, *ACS Catal.* **2015**, *5*, 4260.
[149] S. Nandi, A. S. Nair, B. Pathak, *J. Chem. Sci.* **2019**, *132*, 2.
[150] M. Xiao, L. Gao, Y. Wang, X. Wang, J. Zhu, Z. Jin, C. Liu, H. Chen, G. Li, J. Ge, Q. He, Z. Wu, Z. Chen, W. Xing, *J. Am. Chem. Soc.* **2019**, *141*, 19800.
[151] H. Wang, H. Ren, S. Liu, S. Yin, S. Jiao, Y. Xu, X. Li, Z. Wang, L. Wang, *Chem. Eng. J.* **2022**, *438*, 135539.
[152] J. Hong, S. Hyun, M. Tsipoaka, J. S. Samdani, S. Shanmugam, *ACS Catal.* **2022**, *12*, 1718.
[153] J. Jia, Z. Chen, Y. Liu, Y. Li, J. Zhao, *ACS Appl. Mater. Interfaces* **2020**, *12*, 54517.
[154] H. B. Tao, J. Zhang, J. Chen, L. Zhang, Y. Xu, J. G. Chen, B. Liu, *J. Am. Chem. Soc.* **2019**, *141*, 13803.
[155] C. Zhou, X. Chen, S. Liu, Y. Han, H. Meng, Q. Jiang, S. Zhao, F. Wei, J. Sun, T. Tan, R. Zhang, *J. Am. Chem. Soc.* **2022**, *144*, 2694.
[156] L. Cui, K. Fan, L. Zong, F. Lu, M. Zhou, B. Li, L. Zhang, L. Feng, X. Li, Y. Chen, L. Wang, *Energy Storage Mater.* **2022**, *44*, 469.
[157] X. Peng, S. Zhao, Y. Mi, L. Han, X. Liu, D. Qi, J. Sun, Y. Liu, H. Bao, L. Zhuo, H. L. Xin, J. Luo, X. Sun, *Small* **2020**, *16*, 2002888.
[158] Z. Lyu, X. G. Zhang, Y. Wang, K. Liu, C. Qiu, X. Liao, W. Yang, Z. Xie, S. Xie, *Angew. Chem., Int. Ed.* **2021**, *60*, 16093.
[159] R. Liang, C. Shu, A. Hu, C. Xu, R. Zheng, M. Li, Y. Guo, M. He, Y. Yan, J. Long, *J. Mater. Chem. A* **2020**, *8*, 11337.
[160] B. You, M. T. Tang, C. Tsai, F. Abild-Pedersen, X. Zheng, H. Li, *Adv. Mater.* **2019**, *31*, 1807001.
[161] N.-T. Suen, S.-F. Hung, Q. Quan, N. Zhang, Y.-J. Xu, H. M. Chen, *Chem. Soc. Rev.* **2017**, *46*, 337.
[162] T. Reier, H. N. Nong, D. Teschner, R. Schlögl, P. Strasser, *Adv. Energy Mater.* **2017**, *7*, 1601275.
[163] L. An, C. Wei, M. Lu, H. Liu, Y. Chen, G. G. Scherer, A. C. Fisher, P. Xi, Z. J. Xu, C. H. Yan, *Adv. Mater.* **2021**, *33*, 2006328.
[164] Y. Wen, P. Chen, L. Wang, S. Li, Z. Wang, J. Abed, X. Mao, Y. Min, C. T. Dinh, P. Luna, R. Huang, L. Zhang, L. Wang, L. Wang, R. J. Nielsen, H. Li, T. Zhuang, C. Ke, O. Voznyy, Y. Hu, Y. Li, W. A. Goddard, III, B. Zhang, H. Peng, E. H. Sargent, *J. Am. Chem. Soc.* **2021**, *143*, 6482.
[165] N. B. Halck, V. Petrykin, P. Krtil, J. Rossmeisl, *Phys. Chem. Chem. Phys.* **2014**, *16*, 13682.
[166] Q. Yao, B. Huang, N. Zhang, M. Sun, Q. Shao, X. Huang, *Angew. Chem., Int. Ed.* **2019**, *58*, 13983.
[167] J. Wang, H. Yang, F. Li, L. Li, J. Wu, S. Liu, T. Cheng, Y. Xu, Q. Shao, X. Huang, *Sci. Adv.* **2022**, *8*, eabl9271.
[168] R. Huang, Y. Wen, H. Peng, B. Zhang, *Chin. J. Catal.* **2022**, *43*, 130.
[169] Y. Lin, Z. Tian, L. Zhang, J. Ma, Z. Jiang, B. J. Deibert, R. Ge, L. Chen, *Nat. Commun.* **2019**, *10*, 162.
[170] J. Kim, P. C. Shih, Y. Qin, Z. Al-Bardan, C. J. Sun, H. Yang, *Angew. Chem., Int. Ed. Engl.* **2018**, *57*, 13877.
[171] C. Rong, X. Shen, Y. Wang, L. Thomsen, T. Zhao, Y. Li, X. Lu, R. Amal, C. Zhao, *Adv. Mater.* **2022**, *34*, 2110103.
[172] Y. Yao, S. Hu, W. Chen, Z.-Q. Huang, W. Wei, T. Yao, R. Liu, K. Zang, X. Wang, G. Wu, W. Yuan, T. Yuan, B. Zhu, W. Liu, Z. Li, D. He, Z. Xue, Y. Wang, X. Zheng, J. Dong, C.-R. Chang, Y. Chen, X. Hong, J. Luo, S. Wei, W.-X. Li, P. Strasser, Y. Wu, Y. Li, *Nat. Catal.* **2019**, *2*, 304.
[173] J. Zhu, Y. Guo, F. Liu, H. Xu, L. Gong, W. Shi, D. Chen, P. Wang, Y. Yang, C. Zhang, J. Wu, J. Luo, S. Mu, *Angew. Chem., Int. Ed.* **2021**, *60*, 12328.
[174] S. Xu, J. Hu, L. Huang, Y. Liu, X. Zheng, D. Jiang, *J. Colloid Interface Sci.* **2022**, *615*, 327.
[175] S. C. Sun, H. Jiang, Z. Y. Chen, Q. Chen, M. Y. Ma, L. Zhen, B. Song, C. Y. Xu, *Angew. Chem., Int. Ed.* **2022**, *61*, 202202519.

Xianjun Cao is a Ph.D. candidate in the School of Environmental and Chemical Engineering, Shanghai University, China. She received her Master degree from School of Materials Science and Engineering at Shanghai University. Her research interests focus on the synthesis of functional nanomaterials for electrocatalytic energy conversion.

Yufei Zhao is an associate professor at Shanghai University. She received her Ph.D. dual-degree from Beijing Institute of Technology in 2017 and University of Technology Sydney, in 2018. After receiving her Ph.D., she worked as a postdoctoral research associate at the University of New South Wales, University of Technology Sydney and South China University of Technology. Her research interest focuses on synthesis and application of atomically dispersed catalysts, 1D carbon nanofibers, and 2D graphene-based catalysts for electrocatalytic conversion reactions.

Hao Liu obtained his Ph.D. degree from University of Wollongong in 2011. He worked as a research associate in University of Queensland and moved to University of Technology Sydney as a Chancellor's postdoctoral research fellow. He is a Future Fellow awarded by Australian Research Council. Dr. Liu interests in the synthesis of nanostructured materials and their applications in the fields of lithium-ion batteries, sodium-ion batteries, lithium–sulfur batteries, lithium–oxygen batteries, supercapacitors, and electrocatalysts.

Guoxiu Wang is a Distinguished professor and the Director of the Centre for Clean Energy Technology at University of Technology Sydney. He has been working in the areas of materials science and engineering, materials chemistry, electrochemistry, energy storage and conversion, battery technology, and nanoscience and nanotechnology for over 20 years. He has performed extensive research on electromaterials for applications in rechargeable lithium-ion batteries, lithium–air batteries, sodium-ion batteries, lithium–sulfur batteries, supercapacitors, electrocatalysts, and fuel cells, as well as controllable synthesis of 1D semiconductor nanostructures and their applications.